The Effects of Anthropogenic Electromagnetic Fields on the Behavior of Geomagnetically Displaced Skates

Kyle C. Newton, PhD (1,2)
kylecnewton@gmail.com; ORCID: 0000-0003-1499-0714

Natalie H Donato (3)

Sarah Henkel (2,3)

Taylor K Chapple (1,2)

1 Coastal Oregon Marine Experiment Station, Oregon State University, Newport, OR, USA
2 Department of Fisheries, Wildlife and Conservation Sciences, Oregon State University, Corvallis, OR, USA
3 Department of Integrative Biology, Oregon State University, Corvallis, OR, USA

GRAPHICAL ABSTRACT

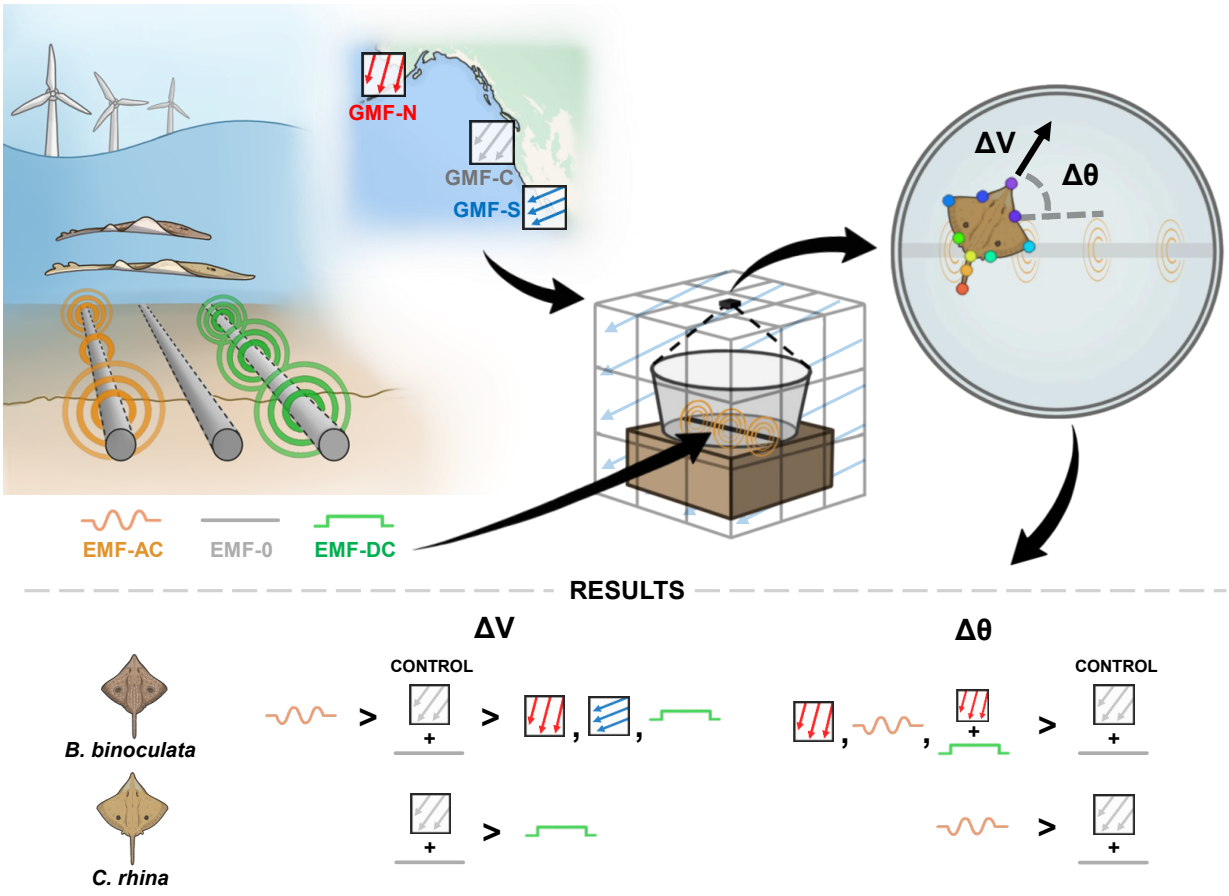

ABSTRACT

To mitigate the effect of climate change, the demand for marine renewable energy infrastructure is increasing worldwide. These facilities convert the kinetic energy of offshore wind, waves, tides or currents into electricity that is transported to shore through alternating current (AC), or direct current (DC), subsea cables. Energized cables emit magnetic fields radially into the surrounding seawater and induce secondary electric field artifacts. Thus, anthropogenic electromagnetic fields (EMFs) can alter the local geomagnetic landscape and may impact the behavior of EMF sensitive elasmobranchs that use the geomagnetic field (GMF) to navigate. We magnetically displaced big (*Beringraja binoculata*) and longnose (*Caliraja rhina*) skates to determine their response to GMF navigational cues. We then exposed skates to model AC and DC subsea cables, to determine their response to fluctuating and constant EMFs, and GMF and EMF to understand how EMF-AC and EMF-DC impacts GMF mediated behaviors. Experiments were recorded on video and 3D pose estimation software tracked the velocity, body angle, and spatial use of skates to quantify their behavioral response to magnetic stimuli. Big skates exposed to GMF and EMF were more active and showed the greatest changes in spatial use, velocity, and body angle. Conversely, longnose skates were less active but showed significant magnetic stimulus-specific changes in their movement kinematics. Thus, skates exposed to GMF and EMF showed stimulus- and species-specific changes in their behavior. Future studies will leverage these lab-based results to interpret the response of free-ranging elasmobranchs to EMF.

INTRODUCTION

To mitigate climate change, the demand for the development and implementation of marine renewable energy (MRE) projects is growing worldwide (Albert et al. 2020, Gill and Desender 2020). These installations convert the kinetic energy of offshore wind, waves, tides, or currents into electricity that is transported back to shore through high voltage subsea cables (HVCs). Depending on the length (typically < 100 km) and purpose of the HVC (e.g., inter-array, export), it will carry electricity in the form of alternating current (AC) that fluctuates back and forth, or direct current (DC), that is constant over time. As electricity is conducted through an HVC, it has been calculated to emit a current-dependent magnetic field of up to 5000 μT (*reviewed in* Albert et al. 2020) radially from the cable for up to several 10s of meters, which can induce secondary electric fields (1-700 μV/m) around animals that swim through them (Figure 1; Newton et al. 2019, Gill and Desender 2020). The intensity of these anthropogenic electromagnetic fields

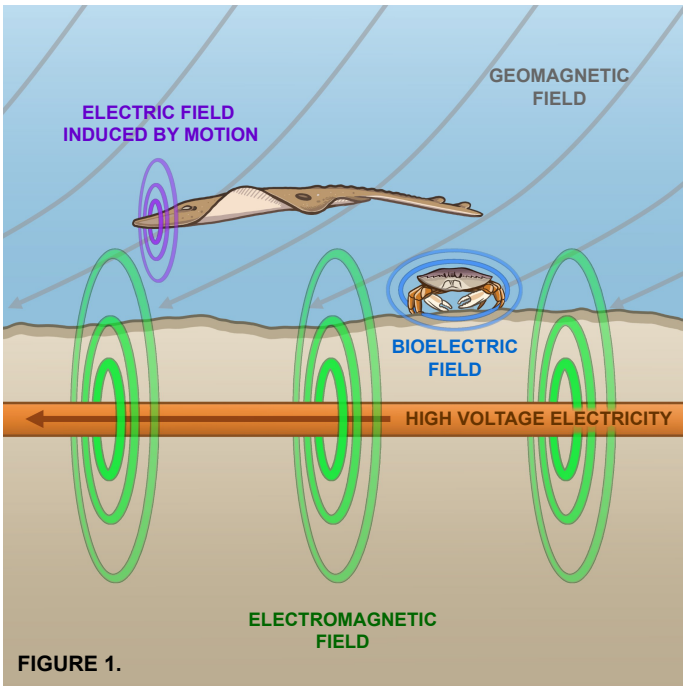

Figure 1. Depiction of natural and anthropogenic magnetic and electric fields encountered by an electroreceptive skate moving across the seabed. The buried subsea cable (orange) conducts electricity along its length. While it is electrically shielded, a magnetic field (green) is emitted radially into the environment. This electromagnetic field (EMF) can alter the local geomagnetic field (gray) and induce secondary electric fields (purple) around an animal (e.g. skate or crab) as it moves through electrically conductive seawater. Thus, EMFs could potentially impact magnetically based navigation behavior or mask bioelectric fields emitted by prey that skates use during foraging.

(EMFs) could be up to 70-150X greater than that of the geomagnetic field (GMF: 20 - 70 μT). Measured magnetic fields from *in situ* seafloor cables range from 0.005 to 150 μT (Albert et al. 2020, Copping & Hemery 2020). Thus, EMFs can potentially alter the local GMF landscape, induce secondary electric fields that mask bioelectric cues, and impact electrically and magnetically mediated behaviors in EMF sensitive species (Albert et al. 2020, Bevelhimer et al. 2013, Gill and Desender 2020, Hutchison et al. 2020 & 2021, Klimley et al 2021, Scott et al. 2021, Woodruff et al. 2013).

Elasmobranch fishes (sharks, skates, rays) use their electroreceptors, the ampullae of Lorenzini, to detect the bioelectric fields of: prey during foraging (Bedore and Kajiura 2013, Kajiura and Holland 2002), conspecifics during the mating season (Tricas et al. 1995, Sisneros et al. 2000), predators during crypsis (Ball et al. 2005, Kempster at al. 2012, Sisneros et al. 1998), and likely to indirectly detect geomagnetic field cues during navigation (Anderson et. al 2017, Kalmijn 1974, 1978, 1988, 2000, Keller et al. 2021, Newton and Kajiura 2020a & 2020b). Physiological studies have shown that elasmobranch electroreceptors are best tuned to detect weak (< 20 nV/cm; Montgomery 1984, Murray 1962, Tricas and New 1998), low frequency (0.5-20 Hz; Adrianov et al. 1984, Peters & Evers 1985, Montgomery 1984, Tricas and New 1998), sinusoidal (AC) electric fields, which corresponds to the bioelectric field stimuli produced by marine organisms as they exchange of ions at the gills and ventilate (Bedore and Kajiura 2013). However, the morphological convergence of multiple receptor afferents onto ascending neurons results in lower behavioral thresholds (< 1 nV/cm) and greater sensitivity to a wide range of stimulus parameters (*reviewed in* Newton et al. 2019).

Similarly, though magnetic stimuli are not generally associated with biological systems and are not known to be naturally attractive to elasmobranchs, physiological studies have shown that their electrosensory system can detect the on- and offset of weak magnetic stimuli. This

response in the thorny skate (*Raja radiata*; Adrianov et al. 1984), common stingray (*Trygon pastinaca;* Adrianov et al. 1984, Akoev et al. 1976, Brown and Ilyinsky 1978), and thornback ray, (*Raja clavata*; Akoev et al. 1976, Brown and Ilyinsky 1978) rapidly attenuates in the presence of static magnetic fields. It has been hypothesized that elasmobranchs could use the GMF to navigate (Kalmijn 1978, 1981, 1982, 1984, 2000, Molteno and Kennedy 2009, Paulin 1995). Scalloped hammerhead sharks (*Sphyrna lewini*) are known to swim along the contours of the weak bathymetric magnetic stimuli produced by ferric compounds in the seafloor and perhaps navigate their environment by magnetic topotaxis (Klimley 1993). Bonnethead sharks (*S. tiburo*) can use experimentally manipulated GMF cues to derive a sense of their current location relative to that of a goal (e.g., a map sense) and maintain the correct heading (e.g., compass sense) to orient towards their home range (Keller et al. 2021). Such GMF-based navigation behavior has never been demonstrated in a batoid (skate or ray), but Uroliphid stingrays can detect the polarity (*Urobatis halleri*; Kalmijn 1978, *U. jamaicenis*; Newton and Kajiura 2020a), intensity and inclination angle (*U. jamaicenis*; Newton and Kajiura 2020b) cues of the GMF.

Elasmobranch magnetic field detection experiments have been conducted on a few species and have begun to describe their general sensitivity (Anderson et al. 2017, Meyer et al. 2005), natural and conditioned behavioral responses to the GMF (Kalmijn 1978, Keller et al. 2021, Newton et al. 2020a & 2020b), permanent magnets (Newton et al., 2017, Polpetta et al. 2021), and the EMF emitted by AC (Albert et al. 2021, Gill et al. 2009, Orr 2016) and DC cables (Albert et al. 2021, Hutchison et al. 2018 and 2020, Orr 2016). Despite inconsistent results across studies, strong permanent magnets (~2000X the GMF intensity) can initially repel sharks and rays from bait but they often become habituated in the absence of reinforcement (O'Connell et al. 2011, 2014a, 2014b, 2014c, 2015, Robbins et al. 2011, Siegenthaler and Jones 2016, Smith and O'Connell 2014, Stoner and Kaimmer 2008). Little skates (*Leucoraja erinacea*) spent more

time near an energized DC cable emitting constant EMFs compared to controls (Hutchinson et al. 2020) and were possibly engaged in unsuccessful foraging behavior. Juvenile thornback rays (*Raja clavata*) were attracted to DC but not AC cables (Albert et al. 2021) while adult thornback rays increased their movement and spotted catsharks (*Scyliorhinus canicula*) spent more time near AC cables (Gill et al. 2009). New Zealand carpet sharks (*Cephaloscyllium isabellum*) were attracted to DC, but not AC cables (Orr 2016).

The behavioral repertoire of an organism is its first line of defense against rapid environmental change, and these studies show that the behavioral responses of elasmobranchs to EMF stimuli can vary significantly depending on the species, life stage, ecological niche, and the quality, magnitude, and duration of stimuli (*reviewed in* Hutchinson et al. 2021, Hermans et al. 2024). Given the breadth of responses, it is possible that an elasmobranch that encounters a rapid and relatively significant (~10X) increase in the local GMF due to an anthropogenic EMF could stop to investigate, bite, turn away from, or ignore the anomaly as they progress along their migratory route (Klimley et al. 2021, Marra et al. 1989, Taormina et al. 2018, Gill and Desender 2020).

Therefore, the imminent expansion of MRE infrastructure and HVC networks requires comprehensive research into the acute and chronic effects that EMF will have on the GMF-based behaviors, such as navigation, of receptive species (Gill and Desender 2020, Hutchinson et al. 2021, Klimley et al. 2021, Newton et al. 2019). The overall intensity (***F***) and inclination angle (***I***) of the GMF changes predictably with latitude such that unique combinations of ***F*** and ***I*** can be used to describe geographic locations on the Earth. GMF-based navigation behavior has been demonstrated in several species (Lohman et al. 1996, Keller et al. 2021, Naisbett-Jones et al. 2017 and 2020, Minkoff et al. 2019, Putman et al. 2014) by manipulating the ambient GMF to “magnetically displace” animals to a geographic location (treatment) that is within their normal distribution but different from their current physical location (control). Currently, there are several

knowledge gaps in quantifying the behavioral response of phylogenetically diverse elasmobranch species exposed to GMF displacement stimuli and EMFs from fluctuating AC and constant DC subsea cables, especially under conditions that test the impact of repeated encounters with HVCs over small spatiotemporal scales (Gill and Desender 2020, Klimley et al. 2021, Gill and Hutchison 2021, Hermans et al. 2024).

This project aimed to determine if the big (*Beringraja binoculata*) and longnose (*Caliraja rhina*) skates show a measurable behavioral response to EMF anomalies emitted by model HVCs. Because elasmobranch electroreceptors are well tuned to detect fluctuating stimuli, we predicted that the EMF emitted from AC cables would elicit stronger responses from skates than the constant EMF emitted from DC cables. However, as the AC output is expected to oscillate at 60 Hz (typical of US installations), it is possible that this higher frequency might make the emitted EMF's less attractive than if they oscillated at < 20 Hz, which might be more biologically relevant. As such, our hypotheses are that skates: (H1) can detect alterations to the ambient GMF, (H2) will alter their behavior in response to GMF displacement, (H3) can detect the EMFs emitted by an AC and DC model HVC, (H4) will alter their behavior in response to EMF cues, and (H5) will alter their GMF response (i.e., H2) with repeated EMF exposure. This work provides a foundation for future broad comparisons across phylogeny and ontogeny as well as longitudinal studies into the cumulative effects of chronic EMF exposure, including those with particular emphasis on vulnerable life history stages for each species (Gill and Desender 2020, Hutchinson et al. 2021, Hermans et al. 2024).

METHODS

Skates

Big skates (n = 4; DW = 30-40 cm) were either captured (n=2) using a 2 m wide benthic beam trawl (44.701°, -124.143°; 35 m depth) or donated (n=2) from local aquaria, and Longnose

skates (n = 3; DW = 50-60 cm) were caught using bottom set long line (43.317°, -129.745°; 310 m depth). Skates were held on the boat deck in flow through seawater tanks then transferred to oxygenated seawater tanks and transported to the laboratory at Hatfield Marine Science Center in Newport, OR. Skates were housed in flow through seawater tanks (2 m dia.) on a 12:12 hr light:dark cycle and fed a mixture of shrimp, clams, herring, and nutritional supplements (Shark and Ray Supplement; Mazuri, SKU 0053065) every other day (7-10% BW / week). Once subjects were feeding for a minimum of 30 days, they were deemed sufficiently acclimated to captivity and healthy for behavioral testing. All procedures were conducted within the ethical guidelines set by the Institutional Animal Care and Use Committee of Oregon State University under protocol #2022-0257.

Experimental Apparatus

The experimental apparatus (Figure 2A-B) was constructed in a magnetically uniform location within the laboratory and consisted of a 1.8 m round polyethylene tank filled to 60 cm placed on a level platform of wooden pallets (~ 1 m high, iron nails removed, topped with a layer of 5 cm foam core) and a model HVC placed within a Merritt coil system (Merritt et al. 1983). The Merritt coils were used to generate geomagnetic field (GMF) pseudo displacement stimuli, whereas the model HVC generated EMF noise stimuli. The Merritt coil system was constructed with 38 mm PVC pipe and fittings (3 x 3 x 3 m overall) and two continuous loops of 14 AWG wire were secured to the PVC structure: one loop was a series of four horizontal loops and the other a series of four vertical loops (26, 11, 11, and 26 windings) that were spaced 1.11, 0.78, and 1.11 m apart. The coils were positioned so that the horizontal and vertical coils were aligned with the vertical and horizontal components of the GMF, respectively. Each loop of the coil system was powered by a single channel 30 W DC power supply (30 V, 5A, Model #TP3005DM, TEK Power, Montclair, CA). A customized configuration of switches and circuitry controlled the

direction and amount of electric current flowing through the coils. The model HVC was

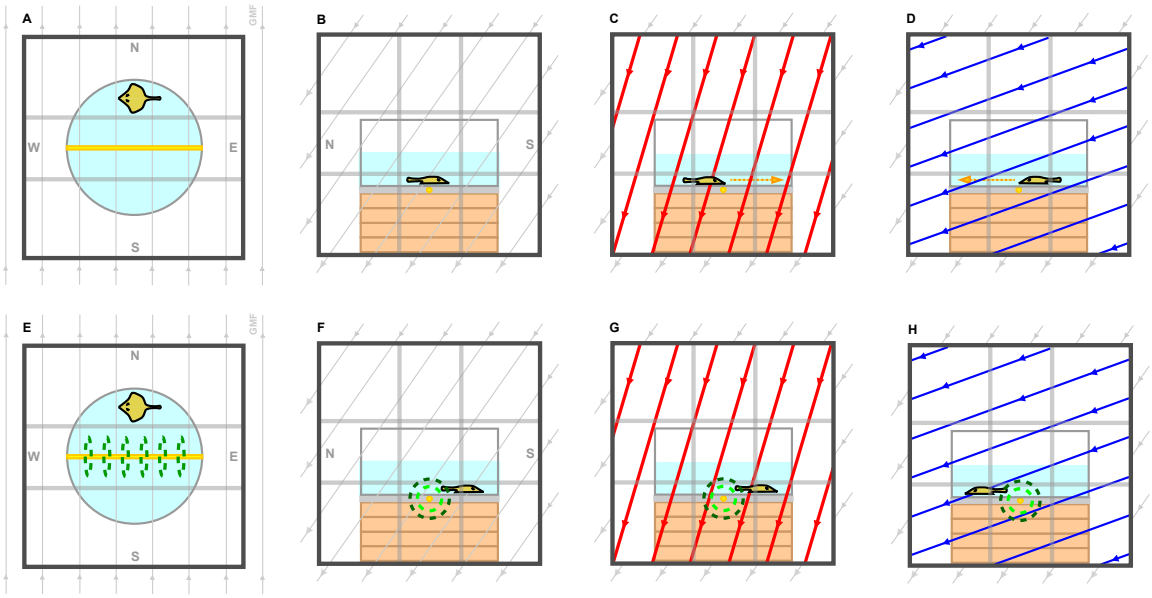

FIGURE 2.

Figure 2. Experimental arena, Merritt Coil system, and mock subsea cable used to conduct geomagnetic field displacement and electromagnetic field exposure trials on big and longnose skates. A) Overhead and B) lateral views of skate in a tank (2 m diameter), direction of ambient geomagnetic field (GMF; light gray arrows), Merritt Coil system (thick gray lines; 3 x 3 x 3 m), mock subsea cable (yellow) emits electromagnetic field noise (EMF; green dotted circles) along west-east axis underneath tank. Mock subsea cable (yellow) located directly under the tank conducted either alternating (AC) or direct (DC) current and emitted fluctuating or constant EMF (green dotted circles), respectively. Cardinal directions indicated with capital letters. Tank was placed on top of wooden pallets to ensure it was within the uniform portion of the altered GMF produced by Merritt Coils during magnetic displacement trials. C) GMF-North displacement trial conditions without EMF noise. Red arrows within Merritt coils indicate altered GMF to match that of geographic location within the northern portion of species distribution. Orange arrow indicates expected southward movement pattern of skate magnetically displaced to the north if it demonstrated a GMF-based bicoordinate map sense. D) GMF-South displacement trial conditions without EMF noise. Blue arrows within Merritt coils indicate altered GMF to match that of southern geographic location within species distribution. Orange arrow indicates expected northward movement pattern of skate if it were magnetically displaced to the south and demonstrated a GMF-based bicoordinate map sense. E) Overhead and F) lateral views of skate during exposure to EMF (dotted green circles) emitted by mock cable. G) GMF-North displacement trials with EMF noise (green dotted circles). H) GMF-South displacement trials with EMF noise (green dotted circles).

constructed of 10 AWG single conductor wire then placed on top of the layer of foam core directly underneath the east-west axis of the tank. A single conductor was chosen because it is the simplest to model for this initial study and creates a foundation for future work with multiple conductors (e.g., three phase AC). Depending on the experiment, the model HVC was connected to an AC (Variac Variable Transformer, model # TDGC2-3D, Circuit Specialists) or DC (60 V, 24A; model #RD6024, AVHzY) power supply. A tri-axial magnetometer (model #3AMG, Alphalab Inc.) and the Physics Toolbox Sensor Suite (www.vieyrasoftware.net) for

mobile devices were used to confirm the uniformity of the ambient GMF within the arena, ***F*** and ***I*** of the resultant GMF pseudo displacement and EMF noise magnetic stimuli.

Geomagnetic and Electromagnetic Field Stimuli

We monitored the changes in spatial use and orientation angle of individuals exposed to altered GMF conditions, to discern if (1) skates can detect GMF cues (H1: e.g., ***F*** and ***I***), (2) alter their behavior, such as: use the GMF to derive a sense of their current location with respect to a goal (H2), and (3) maintain the correct heading to achieve that goal during navigation (H2). If subjects do not respond, it could mean that they either could not detect the stimuli, or that the stimuli were not sufficient motivation to elicit a navigation response. GMF control (GMF-C) stimulus exposure consisted of trials conducted at the ambient GMF in Newport, OR, [***F*** = 51.1 μT (horizontal = 20.6 μT, vertical = 46.9 μT), ***I*** = 66°); Figures 2A-B, E-F]. Geomagnetic north (GMF-N; Figure 2C, G) and south (GMF-S; Figure 2D, H) pseudo displacement stimuli were chosen to mimic the northern (***F*** = 54.6 μT, ***I*** = 73.0°; AK, USA) and southern (***F*** = 41.0 μT, ***I*** = 49.2°; Baja, MX) ends, respectively, of the estimated distribution for both species (Fishbase.se).

The intensity of the EMF stimuli from our model HVC when powered by AC (EMF-AC) fluctuated ± 500 μT at 60 Hz with additional low band oscillations at frequencies of ~ 0.25 and 1 Hz (Figures SI1A, C). Conversely, the EMF stimuli emanated when powered by DC (EMF-DC) had a constant intensity of + 500 μT above the ambient GMF (Figures SI1B, D). The EMF-AC and -DC values were chosen to (1) standardize the relative change in magnetic field stimuli to 10X that of the ambient GMF, (2) remain within the range of magnetic stimuli possible from energized AC and DC HVCs in active MRE farms (Albert et. al 2020), and (3) be strong enough to likely elicit an observable response, if detected by the study organisms. Control EMF stimulus conditions consisted of exposure to the non-energized model HVC that did not emit EMF noise (EMF-0; Figure 2A-D).

Behavioral Trial Procedure

An individual skate was transferred from its husbandry tank into the experimental tank via rubberized net and allowed to acclimate for 10 min. Acclimation time was determined from a minimum of three baseline activity trials (> 60 min) that allowed skates to return to baseline activity levels and align our study with prior work using similar methods on loggerhead sea turtles, *Caretta caretta* (Lohmann et al. 1991), Chinook salmon, *Oncorhynchus tshawytscha* (Putman et al. 2014), European eels, *Anguilla anguilla* (Naisbett-Jones et al. 2017), and bonnethead sharks (Keller et al. 2021).

We tested whether skates had a behavioral response to EMF from AC and DC HVCs and if these stimuli might impact GMF-based navigation behavior. We used a nested block experimental design (Figure SI-2) to account for the variation of repeated measures exposure of individual skates to magnetic stimuli across multiple sessions. Sessions that tested the behavioral response of individual skates to EMF and GMF stimuli were conducted once per day. A session consisted of transferring a skate from its husbandry tank to the experimental tank, allowing it > 10 min to acclimate, then under one GMF condition (GMF-C, GMF-N, or GMF-S) we presented three separate 10-min EMF stimulus trials (EMF-0, EMF-AC, or EMF-DC) in random order (intertrial interval of 60-180 s). Once the three EMF trials were finished for a particular GMF condition, the skate was returned to its husbandry tank and the session concluded for that individual. Once all individuals were tested under that GMF condition, the sessions ended for that day and the skates were allowed to rest for 2-4 days until the next session of trials. This process was repeated so that each individual skate was exposed to every permutation of EMF and GMF treatments (n = 9). Each permutation was conducted 5 times for each animal (total number of trials per skate = 45) to simulate the scenario of a skate using

GMF cues to navigate, then encountering an MRE array and being exposed to EMF multiple times over a relatively short time frame.

Behavioral Data Collection and 3D Markerless Pose Estimation

All trials were recorded onto a 256 GB micro-SD card at the “Standard” camera setting for the GoPro Hero 11 Black (4K resolution, 30 Hz frame rate, 4:3 aspect ratio, “linear” lens setting). Video recordings of trials included 15s before and after the presentation of GMF and EMF stimuli, but there were no observable immediate responses to the onset and offset of magnetic stimuli. Video files were backed up, labeled according to subject and experimental conditions, and pre-processed (e.g., crop to 800 x 800 px, downsample to 1 Mbps without audio) in Adobe Media Encoder (2023). Despite the high video resolution and sampling rate, skates did not show any observable low latency (<10 ms) response to the EMF or GMF stimuli; thus these parameters preserved the integrity of the recorded behavioral responses and reduced computational load. Post-processed files were analyzed using DeepLabCut (DLC) v2.3.0. A curated set of seven videos had 20 frames extracted (automatic, k-means) from each so that 12 unique body parts (nose; anterior, tip, and posterior of left and right pectoral fins; left and right pelvic fins; base, mid and tip of tail) could be labeled and skeleton connections between body parts defined. The annotated frames were used to create a model by training the dataset for 100,000 iterations then confirming that model training (0.34%) and test (0.71%) errors were minimized. Videos were analyzed using the box tracking method and results saved as csv files for analysis in R. Plotted trajectories and videos with overlaid body parts were used to visually confirm tracking efficacy for each trial. Additional detail can be found in Newton et al. (2023) and online (https://github.com/DeepLabCut/DeepLabCut).

Data Analysis

For spatial use analyses, the arena was either divided along the west-east axis into two (north, south) equal hemispherical regions of interest (ROI), or along the perimeter of the tank to create three (north, central, south) equal ROIs of 120° total arc length. The former method was used to test for changes in spatial use under GMF-N or GMF-S displacement, and the latter method was used to delineate three equal ROI, account for the wall association of skates, and test if they were attracted (greater central ROI use) or repelled (greater north or south ROI use) by EMF stimuli.

DLC data files were concatenated into a master file, wrangled, analyzed and figures produced in R Studio using *base* R and the packages *tidyverse*, *dplyr*, *circular*, *zoo*, *spectral*, *lmer*, *bpnreg*, *goeveg*, *stats*, *MuMIn, ggplot2, and viridis*. The raw behavioral response data for each trial was collected as a 30 Hz time series and subject to autocorrelation. Thus, we used Schoener's ratio (Swihart and Slade 1985) to determine the minimum temporal resolution necessary to remove autocorrelation and achieve independent sampling. Thus, the time series of each trial was down sampled at 1-minute intervals resulting in 10 independent data points per trial and autocorrelation removal was confirmed using corAR1 in *nlme*. Response data were checked for normality with *car* and transformed with the appropriate exponents (lambda = 0.25 - 1.2) as determined by *rcompanion*.

To make our data comparable to previous studies (e.g., Lohmann et al. 1996, Putman et al. 2014), we assumed the skates used the first five minutes to discern their GMF displacement or exposure to EMF and the latter five minutes to elicit their angular response. Thus, we investigated the mean angular response of big and longnose skates for the final five minutes of the magnetic trials in R using *circular* and *circ_MLE*. However, traditional circular statistical methods (e.g., Rayleigh test, Watson Wheeler, Akaike Information Criterion) do not allow for repeated measures designs. Therefore, we transformed the mean body angle data from a

circular (i.e., angular) format to their linear sine (*sin* Θ) and cosine (*cos* Θ) components then compared each parameter using the nested generalized linear mixed model (GLMM) described below. We assumed that any magnetic condition with a significant difference in *sin* Θ or *cos* Θ from that of the appropriate reference condition meant that the corresponding body angles for those conditions were different as well. Because our frame of reference used 0° to indicate north, and using the definitions of trigonometric functions, the *sin* Θ values were interpreted to indicate significant changes in body angle along the east-west axis, whereas *cos* Θ values indicated changes along the north-south axis.

To examine how the behavioral response of skates might vary during exposure to EMF and GMF stimuli, the spatial use (ROI) data were converted to counts then analyzed using a GLMM in R (package *lmer*; e.g., Count ~ ROI * EMF * GMF + (1 | individual), see Tables 1-6). Likewise, the mean velocity and body angle data were analyzed using a GLMM (e.g., response variable ~ EMF * GMF + (1 | individual / session / trial), see Tables 7-20). The GLMM models included terms for the main effects of EMF, GMF, ROI (if necessary), and their interactions. A random effects term nested the multiple independent trial data points within each session and multiple sessions within individual skates to mitigate against pseudo replication from the repeated measures of the nested design. A pseudo R^2 value for GLMMs was generated by *MuMin* to explain the variance of the fixed and random effects. ANOVA type II (Wald) and III (Chi Square) tests were used to determine significance levels for fixed main and interaction effects. Tukey's pairwise comparisons between EMF and GMF were done posthoc using *emmeans* with the appropriate p-value adjustments. A significance level of *alpha* = 0.05 was used for all statistical comparisons. The final statistical models, their output (Tables 1-20), datasets, and R scripts with detailed analyses are located online in the Open Science Framework data repository. (https://osf.io/azydm/; DOI 10.17605/OSF.IO/Z4J9G).

RESULTS

Spatial Use

We predicted that skates displaced to the north would prefer to occupy the southern half of the arena and skates displaced to the south would prefer the northern half. However, the mean spatial use of the arena by big and longnose skates was not significantly different between the northern and southern hemispherical ROI when individuals were exposed to ambient or GMF-N and GMF-S pseudo displacement conditions (Figures 3A-C & 4A-C) under EMF-0.

Among the three edge regions of the tank, under GMF-control there was a significant fixed effect of greater mean use of the central third ROI than the northern or southern third ROI by big and longnose skates in all treatments (EMF-0; Figures 3A & 4A, Tables 1 & 2, EMF-AC; Figures 3D & 4D, Tables 3 & 4, and EMF-DC; Figures 3G & 4G, Tables 5 & 6). Longnose skates did not show a preference for the northern vs. southern third ROIs under any EMF condition (Figure 4), save for GMF-S displacement without EMF (Figure 4C). Conversely, big skates used the northern more than the southern third ROI under GMF-C and all EMF conditions (Figure 3A, D, G) and under GMF-N with EMF-AC and EMF-DC (Figure E, H), but not GMF-N without EMF (Figure 3B) or under GMF-S displacement and all EMF conditions (Figure 3C, F, I). Thus, within a given GMF condition, the general pattern of spatial use within skates did not change with EMF exposure, except when GMF-N displaced big skates and GMF-S displaced longnose skates without EMF were exposed to EMF-AC and EMF-DC.

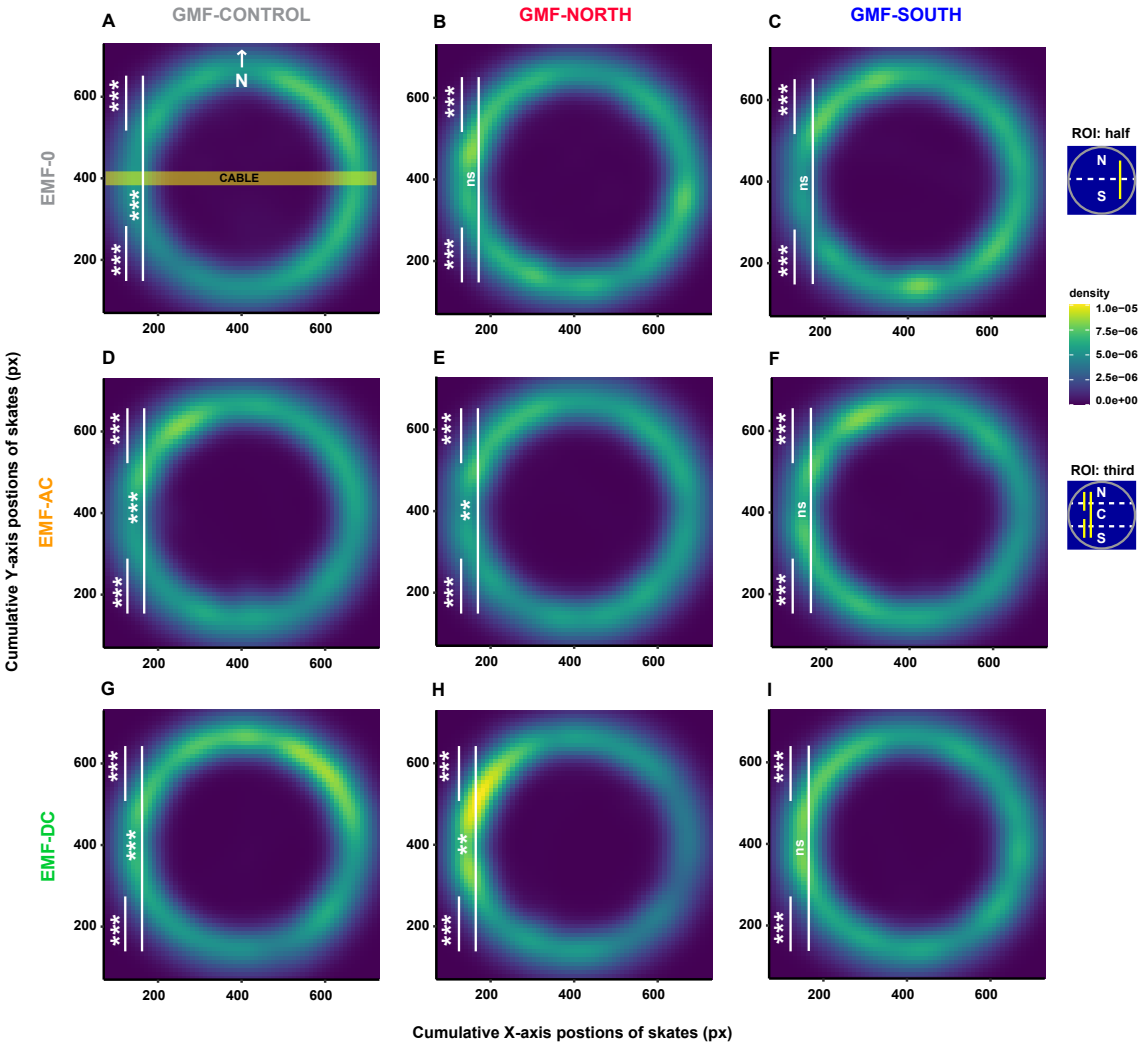

FIGURE 3.

Figure 3. Cumulative spatial use of the arena by big skates during exposure to geomagnetic displacement and electromagnetic noise stimuli. Icons on the upper right of the figure depict regions of interest (ROI) within the arena for statistical comparisons between spatial use of each set. Bars on the left side of panels indicate statistical comparisons between the three northern, central, and southern third ROI to test if skates were attracted or repelled from the central ROI during exposure to EMF noise stimuli. Big skates preferred to use the central third ROI more than the northern and southern third ROI, and the northern more than the southern third ROI during all GMF-C conditions (A, D, G), and GMF-N with EMF (E, H), but not GMF-N without EMF (B) or all GMF-S (C, F, I) displacement conditions. The spatial use of the arena by big skates did not differ between the northern and southern hemispherical ROI during A) GMF-C, B) GMF-N, and C) GMF-S displacement conditions without EMF. Significance values: # = 0.1, * = 0.05, ** = 0.01, *** = 0.001.

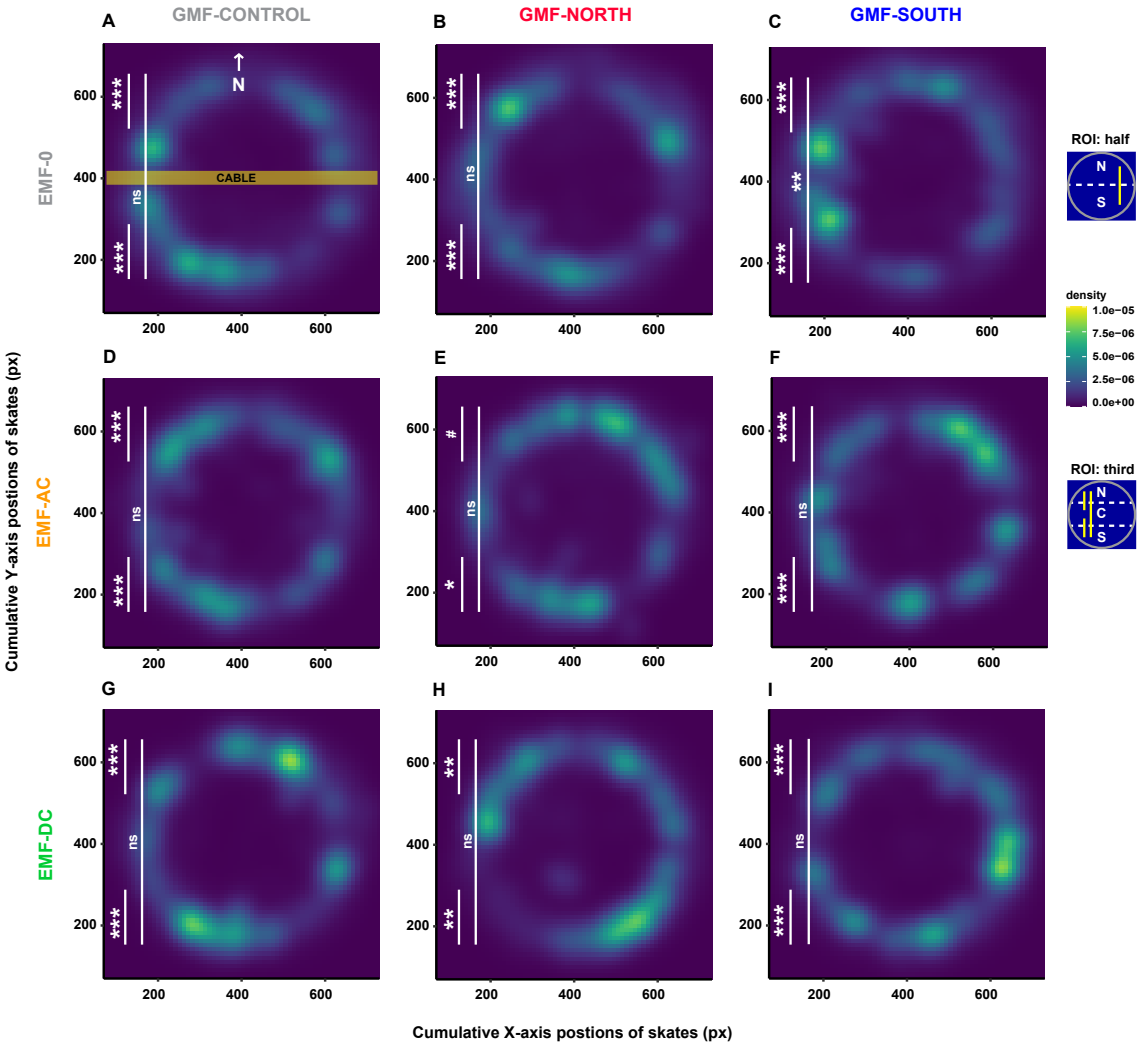

FIGURE 4.

Figure 4. Cumulative spatial use of the arena by longnose skates during exposure to geomagnetic displacement and electromagnetic noise stimuli. Icons on the upper right of the figure depict regions of interest (ROI) within the arena for statistical comparisons between spatial use of each set. Bars on the left side of panels indicate statistical comparisons between the three northern, central, and southern third ROI to test if skates were attracted or repelled from the central ROI during exposure to EMF noise stimuli. Longnose skates preferred to use the central third ROI more than the northern and southern third ROI, which were used equally during all GMF and EMF conditions, save during GMF-S displacement without EMF (C). The spatial use of the arena by big skates did not differ between the northern and southern hemispherical ROI during A) GMF-C, B) GMF-N, and C) GMF-S displacement conditions without EMF. Significance values: # = 0.1, * = 0.05, ** = 0.01, *** = 0.001.

Mean Velocity

The mean velocity of big skates showed significant fixed main effects of EMF, GMF exposure and their interaction (Figure 5, Table 7). In big skates, the main effect of GMF displacement relative to GMF-C conditions (mean ± SE = 8.31 ± 2.53 cm/s) was a significant reduction of their mean velocity during GMF-N (-12.1%) and GMF-S (-10.7%) displacement (Figure 5A, Table 8). Pairwise post hoc comparisons indicated that the effects of GMF-N and GMF-S were primarily realized under EMF-0 conditions, not during EMF-AC or EMF-DC exposure (Table 9).

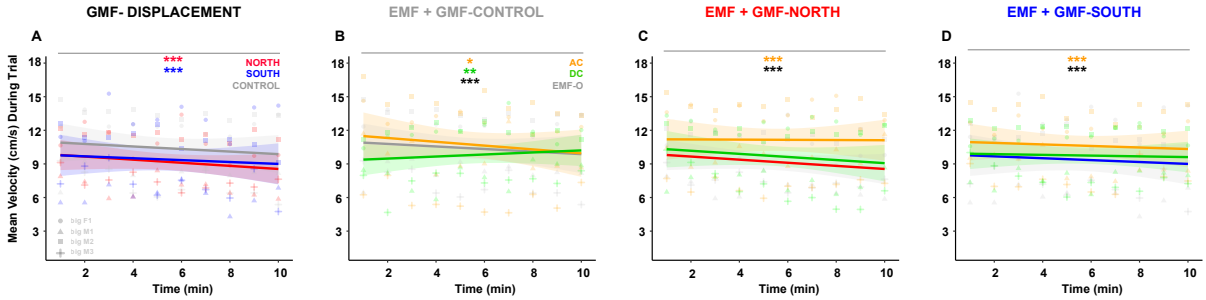

FIGURE 5.

Figure 5. The mean velocity of big skates during exposure to GMF displacement, EMF alone, and EMF during GMF displacement. Big skates had: A) a significantly greater mean velocity during control trials (gray) compared to during GMF-N (red) or GMF-S (blue) displacement trials; B) a significantly greater mean velocity during EMF-AC trials (orange) compared to controls (gray), which had greater velocity compared to EMF-DC (green) trials under ambient GMF (control); C) a significantly greater mean velocity during EMF-AC trials (orange) compared to controls (red) and EMF-DC (green) trials under GMF-N displacement; and D) a significantly greater mean velocity during EMF-AC trials (orange) compared to controls (blue) and EMF-DC (green) trials under GMF-S displacement. Control trials (red and blue lines) during (C) GMF-N and (D) GMF-S displacement are the same as those of (A) GMF displacement without EMF. Significance values: # = 0.1, * = 0.05, ** = 0.01, *** = 0.001. Red symbols compare GMF-N to GMF controls, blue symbols compare GMF-S to GMF controls, orange symbols compare EMF-AC to EMF-0, green symbols compare EMF-DC to EMF-0, black symbols compare EMF-AC to EMF-DC.

The main effect of EMF stimulus on big skates relative to that of EMF-0 controls was a significant increase in mean velocity during EMF-AC (+5.5%) exposure and decrease during EMF-DC (-7.4%) exposure (Table 8). Pairwise post hoc comparisons showed this pattern held under GMF-C conditions (Figure 5B, Table 10). Exposing big skates to EMF stimuli during GMF displacement resulted in significant fixed interaction effects on their mean velocity (Table 6). During GMF-N displacement, the velocity was significantly greater due to interactions with both EMF-AC and EMF-DC (~12.5%) exposure relative to the GMF-C, EMF-0 control condition

(Figures 5A & C, Table 8). However, pairwise post hoc comparisons within GMF-N displacement indicated big skate velocity was significantly greater during EMF-AC exposure compared to EMF-DC and EMF-0, while EMF-DC and EMF-0 were not different from each other (Figure 5C, Table 10). During GMF-S displacement, exposure to EMF-AC had no effect on the mean velocity big skates but exposure to EMF-DC had a significant interaction that resulted in greater (+11.2%) mean velocity relative to the GMF-C, EMF-0 control condition (Figures 5A & D, Table 8). As with GMF-N displacement, pairwise post hoc comparisons showed that the velocity of GMF-S displaced big skates was significantly greater during EMF-AC exposure compared to EMF-DC and EMF-0 while EMF-DC and EMF-0 did not differ (Figure 5D, Table 10).

Longnose skates showed a significant main effect of EMF but no significant main effect of GMF; thus, there was no interaction between EMF and GMF (Figure 6, Table 11). The lack of a main effect on the velocity of longnose skates by GMF displacement was supported by no significant difference in their mean velocity under GMF-N (-5.5%) and GMF-S (-6.5%) displacement relative to GMF-C conditions (mean ± SE = 1.86 ± 0.29 cm/s; Figure 6A, Table 12).

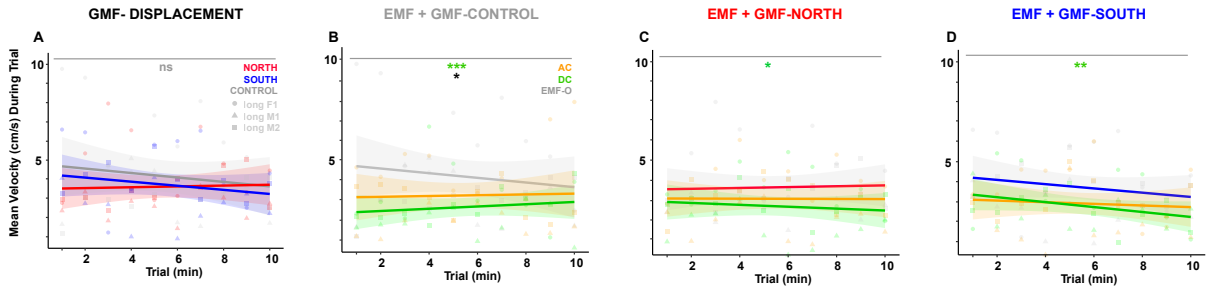

FIGURE 6.

Figure 6. The mean velocity of longnose skates during exposure to GMF displacement, EMF alone, and EMF during GMF displacement. Longnose skates had: A) no significant difference in mean velocity during control (gray), GMF-N (red), or GMF-S (blue) displacement trials; B) a significantly greater mean velocity during control (gray) compared to EMF-AC (orange) trials, and during EMF-AC compared to EMF-DC (green) trials under ambient GMF (control); C) a significantly greater mean velocity during controls (red) compared to EMF-DC (green) trials under GMF-N displacement; and D) a significantly greater mean velocity during controls (blue) compared to EMF-DC (green) trials under GMF-S displacement. Control trials (red and blue lines) during (C) GMF-N and (D) GMF-S displacement are the same as those of (A) GMF displacement without EMF. Significance values: # = 0.1, * = 0.05, ** = 0.01, *** = 0.001. Red symbols compare GMF-N to GMF controls, blue symbols compare GMF-S to GMF controls, orange symbols compare EMF-AC to EMF-0, green symbols compare EMF-DC to EMF-0, black symbols compare EMF-AC to EMF-DC.

Likewise, there were no significant differences in the pairwise post hoc comparisons among all GMF conditions without EMF exposure. The main effect of EMF on longnose skates was a significant reduction in mean velocity during exposure to EMF-DC (-22.9%) and a large but statistically non-significant reduction in velocity during EMF-AC (-9.6%) exposure (Figure 6B, Table 12). Pairwise post hoc comparisons showed significant reductions in the mean velocity of longnose skates during EMF-DC exposure compared to EMF-AC and EMF-0 controls under each of the GMF conditions (Figure 6B-D, Table 13).

Mean Body Angle

The distribution of mean body angles for big skates under the GMF-C, EMF-0 control condition was unimodal and oriented at 17.2° (0° = north) during the final five minutes of trials (Figure 7A). During GMF-N and GMF-S displacement, the distributions became more uniform (Figures 7B, C). When exposed to EMF-AC, the distribution of mean body angles became bimodal and oriented at 338° and 155° (Figure 7D), while during EMF-DC exposure, the distribution of angles was uniform (Figure 7G). Under GMF-N displacement, the distribution was bimodal during EMF-AC (132°, 315°; Figure 7E) and unimodal during EMF-DC (298°; Figure 7H) exposure. Under GMF-S displacement, the distribution was uniform during EMF-AC (Figure 7F) and became unimodal during EMF-DC (235°; Figure 7H) exposure.

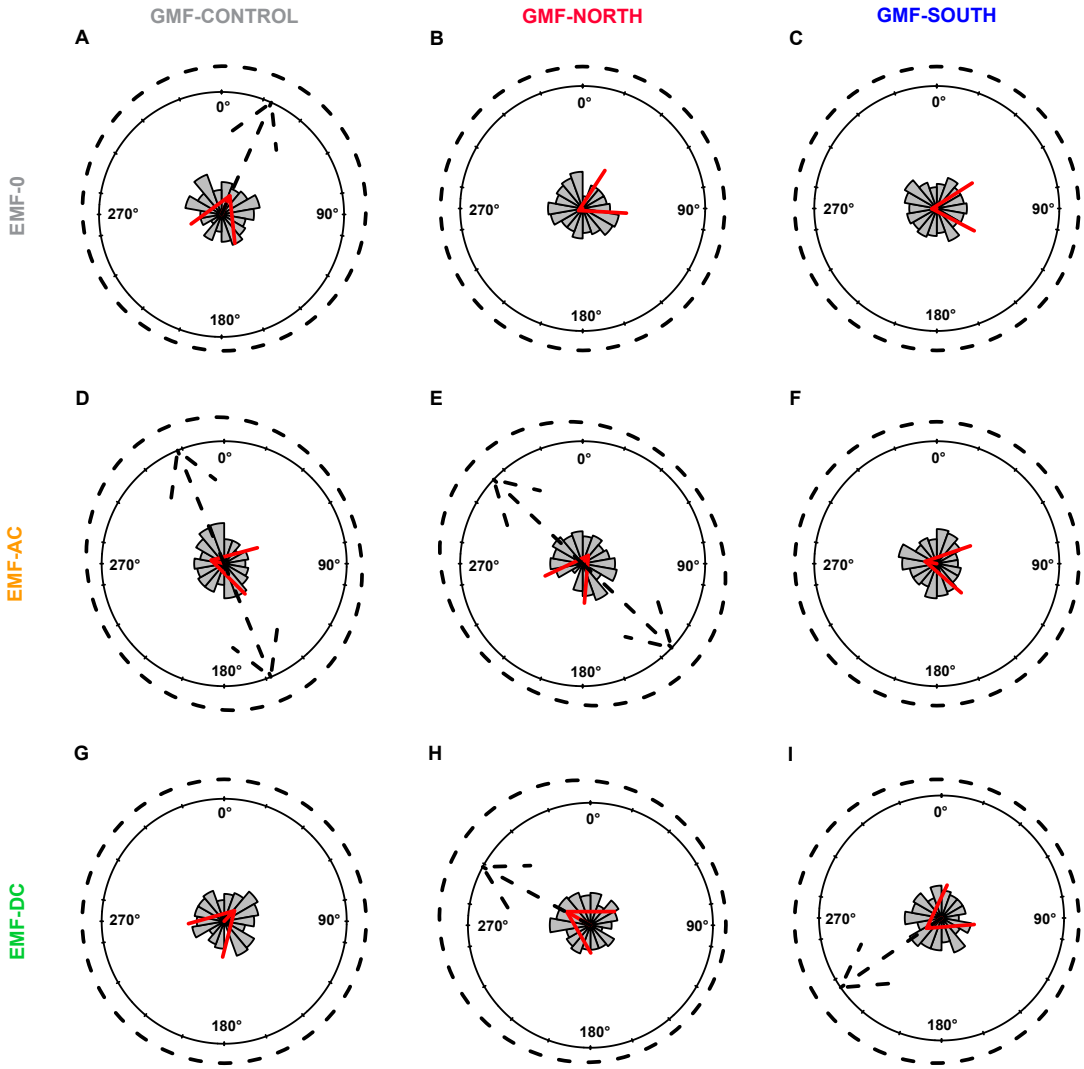

FIGURE 7.

Figure 7. The mean body angle of big skates during the latter half of trials that exposed them to GMF displacement, EMF alone, and EMF during GMF displacement. Polar histograms indicate the relative number of body angle observations within 20° bins, red arrows indicate the mean angle of all the observations, black dotted lines and arrows indicate the density and mean direction, respectively, of the best model of the distribution calculated by the *cric_MLE* package in R. The distribution of the mean body angle of big skates was unimodal under A) GMF-C and EMF-0, uniform under B) GMF-N and C) GMF-S displacement, bimodal under D) EMF-AC exposure and E) GMF-N displacement and EMF-AC exposure, uniform under F) GMF-S displacement and EMF-AC exposure, uniform under G) EMF-DC exposure, and unimodal under H) GMF-N and EMF-DC exposure, and unimodal under I) GMF-S displacement and EMF-DC exposure.

Under GMF-C and EMF-0 control conditions, the distribution of mean body angles for longnose skates was bimodal and oriented at 350° and 23° during the final five minutes of trials (Figure 8A). The distributions became unimodal during GMF-N displacement (0.4 rad; Figure 8B) and bimodal during GMF-S displacement (338°, 189°; Figure 8C). When exposed to EMF-AC, the

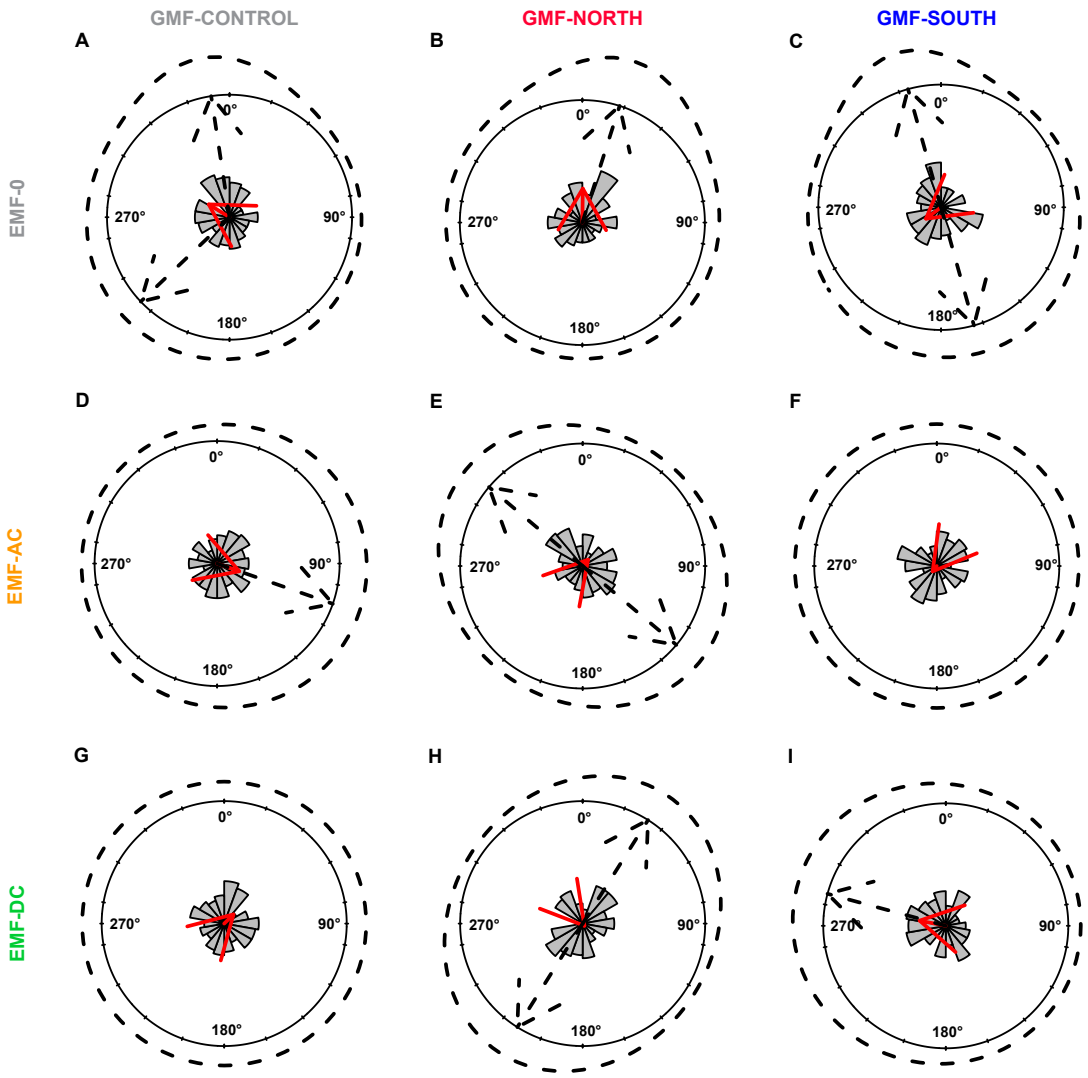

FIGURE 8.

Figure 8. The mean body angle of longnose skates during the latter half of trials that exposed them to GMF displacement, EMF alone, and EMF during GMF displacement. Polar histograms indicate the relative number of body angle observations within 20° bins, red arrows indicate the mean angle of all the observations, black dotted lines and arrows indicate the density and mean direction, respectively, of the best model of the distribution calculated by the *cric_MLE* package in R. The distribution of the mean body angle of longnose skates was bimodal under A) GMF-C and EMF-0, unimodal under B) GMF-N displacement, and bimodal under C) GMF-S displacement, unimodal under D) EMF-AC exposure, bimodal under E) GMF-N displacement and EMF-AC exposure, uniform under F) GMF-S displacement and EMF-AC exposure, uniform under G) EMF-DC exposure, and bimodal under H) GMF-N and EMF-DC exposure, and unimodal under I) GMF-S displacement and EMF-DC exposure.

distribution of mean body angles became unimodal and oriented at 109° (Figure 8D), and during EMF-DC exposure, the distribution became uniform (Figure 8G). Under GMF-N displacement the distribution was bimodal during EMF-AC (120°, 309°; Figure 8E) and bimodal during EMF-

DC (120°, 390°; Figure 8H) exposure. Under GMF-S displacement, the distribution was uniform during EMF-AC (Figure 8F) and unimodal during EMF-DC (286°; Figure 8H) exposure.

The *sin* Θ (variation on east-west axis) of big skates showed significant fixed main effects of GMF displacement, EMF stimuli, their interaction (Table 14) and several pairwise comparisons (Tables 15-17). However, the *cos* Θ data (variation on north-south axis) for big skates showed no fixed effects for GMF, EMF, or their interaction and will not be discussed further. The main effect of GMF displacement on the mean body angle of big skates relative to GMF-C conditions (mean ± SE = 0.05 ± 0.02 rad; Figure SI-3A), was a significant reduction in *sin* Θ during GMF-N (-4.6°) and GMF-S (-4.1°) displacement (Table 15). Pairwise post hoc comparisons showed that under EMF-0 conditions, the main effect of GMF-N on the mean body angle of big skates was due to a significant difference in *sin* Θ (Table 16). The main effect of EMF stimuli on the mean body angle of big skates compared to EMF-0 controls (mean ± SE = 2.9° ± 1.1°; Figure SI-3B) was a significant reduction in *sin* Θ during EMF-AC (-5.2°) but not EMF-DC (-1.7°) exposure (Table 15). Pairwise post hoc comparisons indicated that the main effect of EMF-AC relative to EMF-0 on the mean body angle of big skates under ambient GMF-C conditions was due to a significant difference in *sin* Θ (Table 17). Big skates exposed to EMF stimuli during GMF displacement had a significant fixed interaction effect on mean body angle (Table 14) due to an increase in *sin* Θ of GMF-N displaced skates exposed to EMF-AC (+6.3°, Table 15). Pairwise comparisons showed that this increase was because the *sin* Θ for GMF-N displaced big skates exposed to EMF-AC was significantly greater than during EMF-DC exposure but less than during EMF-0 conditions (Table 17). Under GMF-S displacement, there was no significant effect of EMF stimuli (Table 17). During EMF-AC exposure, there was no significant effect of GMF displacement, but during EMF-DC exposure *sin* Θ was significantly reduced under GMF-N displacement compared to GMF-S and GMF-C conditions (Table 16). Therefore, the main effect

515 of GMF-S was due to a significant reduction in *sin* Θ between GMF-N and GMF-S displaced big
516 skates exposed to EMF-DC (Table 16).
517
518 The *sin* Θ of the mean body angle of longnose skates showed no significant fixed main effects
519 of GMF displacement, EMF stimuli, their interaction and will not be discussed further. The *cos* Θ
520 data for longnose skates showed a significant fixed main effect of EMF; however there was no
521 effect of GMF or their interaction (Table 18). There was a main effect of EMF on the mean body
522 angle of longnose skates due to a significant change in *cos* Θ during EMF-AC exposure (-8.2°)
523 relative to EMF-0 controls (mean ± SE = 5.7 ± 2.9°; Table 19). Pairwise comparisons showed
524 that this effect was primarily due to a significant difference between EMF-AC and EMF-0
525 controls during ambient GMF-C conditions, and a large, but not statistically significant,
526 difference between EMF-AC and EMF-DC during GMF-S displacement (Table 20). There was
527 no effect of EMF during GMF-N displacement.
528
529 **DISCUSSION**
530 We tracked the spatial use, mean velocity, and mean body angle of skates within the
531 experimental tank to quantify their behavioral response to the electro- and geomagnetic stimuli.
532 Although there was no consistent response across species for each metric, we found that big
533 and longnose skates could detect and respond to GMF displacement stimuli (H1, H2), the EMFs
534 emitted by energized AC and DC cables (H3, H4), and exposure to EMF during GMF
535 displacement altered their GMF-evoked behavioral responses (H5). The significant changes in
536 spatial use, mean velocity, and mean body angle are summarized into general trends for each
537 species in Figure 9.
538
539 In response to GMF-N and GMF-S displacement without EMF, neither species of skate
540 significantly altered their preference for the northern or southern hemispherical ROI relative to

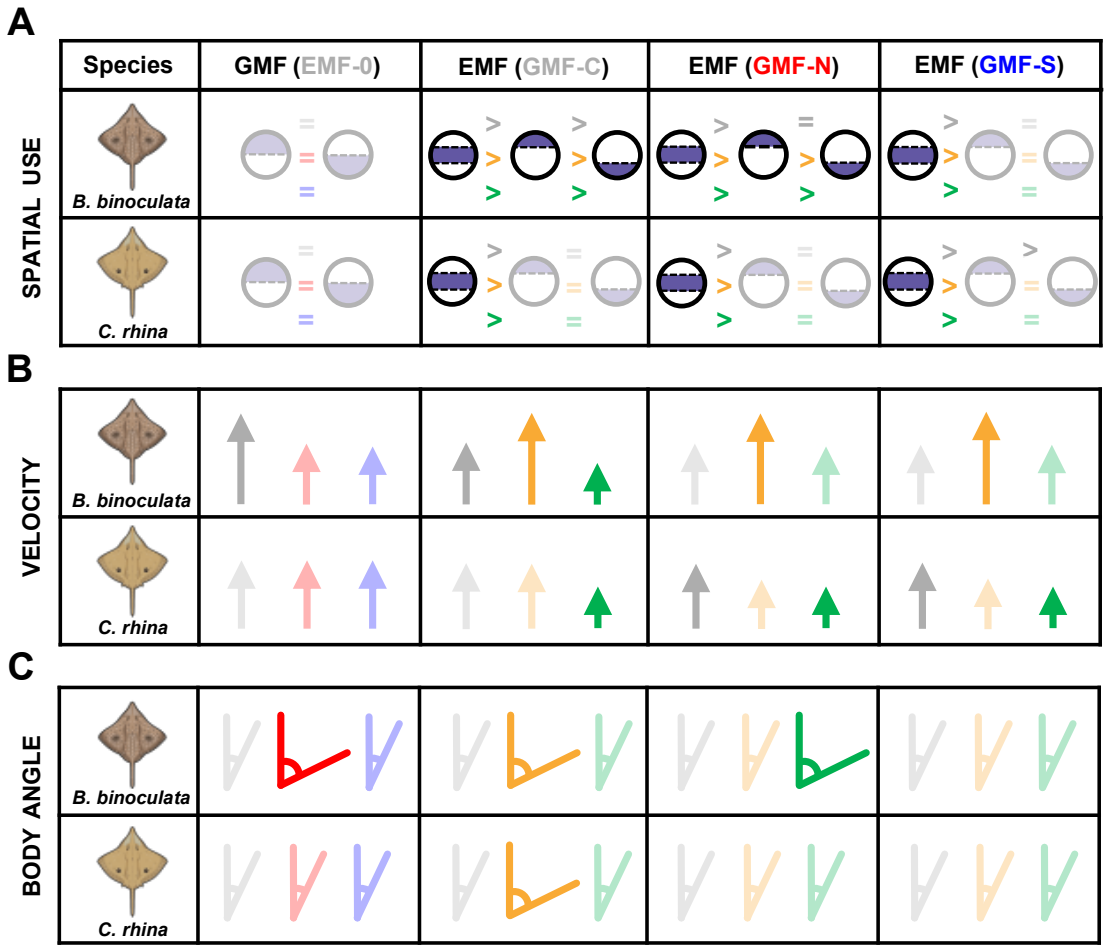

541 **FIGURE 9.**

542 **Figure 9. Summary of the main results for the effect of EMF exposure on GMF displaced skates**. Icon color indicates EMF
543 exposure (gray = no EMF, orange = EMF-AC, green = EMF-DC), or GMF displacement (gray = GMF-C, red = GMF-N, blue = GMF-
544 S) conditions. A) Circular icons indicate the use of the experimental arena divided into halves (GMF + (EMF-0)) or thirds (EMF +
545 (GMF-C, GMF-N, GMF-S)) and mathematical symbols indicate equal use (=) or greater use (>) of a given region relative to another.
546 The relative size of arrow and angle icons indicates the relative magnitude of the B) mean velocity or C) change in mean body
547 angle. Solid icons indicate treatments that differed statistically ($p \leq 0.05$) and translucent icons indicate those that did not differ
548 within a given condition.
549

550 GMF-C conditions (Figure 9), which does not support our prediction that displaced skates would
551 occupy different portions of the tank. As the GMF displacement stimuli within the arena were
552 uniform; GMF sensitive animals would be required to physically move to reorient their sensory
553 array, sample the altered GMF cues from a variety of perspectives, and better get their bearings
554 (Wiltschko and Wiltschko 2007). As such, our findings of no alteration of spatial use of
555 hemispherical ROI during GMF-N and GMF-S displacement relative to GMF-C conditions might

556 indicate that the constraints imposed by our available facilities and acquiring skates of
557 sufficiently small size impacted the spatial and directional responses of skates. Relatively large
558 skates confined to swimming in a mesocosm might not be reliable indicators of GMF-based
559 orientation and navigation behavior as reported by previous authors using vertebrates of smaller
560 size (Lohmann et al. 1996, Naisbett-Jones et al. 2017, Putman et al. 2014), including juvenile
561 bonnethead sharks (Keller et al. 2021) with a total length commensurate to that of our skates.
562
563 Under all GMF and EMF conditions, both species of skates preferred the central ROI over the
564 northern and southern thirds. The lack of change in spatial use across all EMF conditions
565 indicates that relatively strong EMF (~10x GMF intensity) from AC and DC cables did not repel
566 skates away from the EMF source in our mesocosms. However, since the skates preferred the
567 central ROI even under control conditions, we cannot discern if the skates were attracted to the
568 cable, as has been demonstrated with little skates that spent more time near an energized DC
569 cable (Hutchinson et al. 2020), the juvenile Lake sturgeon (*A. fulvescens*, Bevelhiemer et al.
570 2013) and spotted catsharks (*Scyliorhinus canicula*, Gill et al. 2009) that spent more time near
571 AC cables, and was hypothesized as a possibility in green sturgeon (*Acipenser medirostris*,
572 Wyman et al. 2023) and juvenile Chinook salmon (Wyman et al. 2018) that took more time to
573 transit an area with an energized DC cable. Interestingly, the GMF-N displaced big skates and
574 GMF-S displaced longnose skates altered their distribution relative to controls when EMF-AC
575 and EMF-DC were presented. As the interaction between GMF and EMF stimuli prompted each
576 species to respond differently than under control conditions, this likely demonstrates the
577 detection of, and response to, GMF displacement stimuli (H1, H2) can be altered in the
578 presence of EMF (H5).
579
580 In our constrained mesocosm, the orientation of an organism may be a better metric for scoring
581 directional preference rather than the spatial use of the arena (e.g. Minkoff et al. 2020, Naisbett-

Jones et al. 2020). However, while under each of the GMF treatments the distribution of mean body angles for longnose skates varied with EMF treatment, the pattern of relative change in mean body angle of our skates exposed to GMF and EMF showed no clear signal. While the body angle responses did not support our hypothesis of north displacement motivating skates to orient southward (and vice versa), together these results might indicate a generalized change in body angle of skates to EMF stimuli that becomes reduced during GMF displacement conditions.

The velocity responses to altered geo- and electromagnetic fields had a clearer signal than spatial use and/or angle responses (Figure 9). Under GMF-N and GMF-S displacement big skates reduced their mean velocity relative to GMF-C. This pattern was also observed in longnose skates, but neither change was statistically significant perhaps because, under control conditions, longnose skates were less active overall (V_{mean} = 3.2 cm/s ± 0.1 SE) compared to big skates (V_{mean} = 10.1 cm/s ± 0.1 SE). Across all GMF conditions, big skates had the greatest velocity when exposed to EMF-AC. During GMF-C, big skate velocity was lowest under EMF-DC, but there was no difference between EMF-0 and EMF-DC conditions during GMF-N and GMF-S displacement. Across all GMF conditions, longnose skates had the lowest velocity when exposed to EMF-DC. During GMF-C, longnose skate velocity was lower than both EMF-0 and EMF-AC; however, under GMF-N and GMF-S displacement, there was no difference between AC and DC. Thus, for both big and longnose skates, the patterns of change in mean velocity observed under GMF-C were altered in the same fashion under GMF-N and GMF-S displacement. Similar reduction of activity in the presence of an energized DC cable has been observed in the field in little skates (Hutchison et al. 2020), juvenile Chinook salmon (Wyman et al. 2018) and green sturgeon (Wyman et al. 2023) .

If the ampullae of Lorenzini are the primary detectors of magnetic stimuli (Adrianov et al. 1974, 1984, Akoev et al. 1976, Brown and Ilyinsky 1978), then their attunement to the onset and offset of stimuli might make them better suited to detecting and mediating responses to fluctuating AC compared to DC magnetic fields, especially for less active species such as longnose skates. We originally hypothesized that the low frequency components of our EMF-AC stimuli might make the induced electric fields attractive to skates because they might be perceived somewhat similar to the fluctuating weak bioelectric fields emitted by the ion exchange and sinusoidal ventilation mechanism of respiring prey (Bedore et al. 2013). However, the relatively high intensity of the fluctuating EMF-AC used in this study (± 500 μT) might have made the induced electric stimuli less biologically relevant and more overwhelming to big skates, which could explain why they maintained an elevated swimming velocity and had greater changes in the east-west component of their mean body angle distribution under EMF-AC across all GMF conditions. This possibility aligns with the more aversive responses among the greater repertoire of Lake sturgeon responses (e.g., pectoral fin flare, reduced velocity, sudden stops, rapid turns, escapes, body spasms) to strong (> ± 1000 μT) EMF-AC stimulus exposure (Bevelhimer et al. 2013).

Conversely, the temporal stability of constant EMF-DC could have allowed big and longnose skates, once they reduced their velocity, to detect minute GMF displacement stimuli and elicit directed changes in body angle to the west, as seen in the shifts toward unimodal and bimodal angular distributions. For species located along the western coastline of the United States, this might indicate an offshore movement into deeper water. If so, this could imply that big skates under the “navigational pressure” induced by GMF-N displacement could respond more predictably, or intentionally, when they encounter EMF-DC cables compared to EMF-AC which might elicit more of an escape response (higher velocity, greater deviation in angle distribution from control) that could be inshore or offshore.

The reduced velocity and more uniform angular distribution responses of big skates to constant stimuli (i.e., GMF-N, GMF-S, and EMF-DC) and longnose skates to EMF-DC align with the reduced velocity and increased turning behavior seen in little skates exposed to the constant EMF from energized DC cables in the field and could indicate searching behavior (Hutchison et al. 2020). Prior studies have shown that gray bamboo sharks can categorize visual stimuli into groups (Fuss et al. 2014, 2017; Schluessel et al. 2014). Because elasmobranchs have similar neural substrates, it is likely that batoid skates and rays can also categorize environmental stimuli, such as magnetic fields, into groups. If so, then it is possible that big skates recognized the constant GMF and EMF-DC stimuli as similar, perceived them as “magnetic displacement,” and responded to both magnetic stimuli by slowing down and increasing their turning behavior to sample ambient magnetic fields and get their bearings (e.g., Lohmann et al. 1996, Putman et al. 2014).

Conclusions

We found that big and longnose skates respond to electro- and geomagnetic stimuli in species-specific ways. Our data suggest that if free swimming big skates encountered anthropogenic EMF-DC in the field, they might exhibit a greater change in behavior compared to EMF-AC, similar to the investigation behavior (reduced velocity, increased turning) seen in little skates (Hutchison et al. 2020). Conversely, if longnose skates encountered EMF in the field, they might elicit distinct behavioral responses depending on if they encountered EMF-AC in their home range (GMF-C; increased turning), or EMF-DC (reduced velocity) during a migration (GMF-N or GMF-S). Such a distinction might arise if a migrating, or GMF displaced, longnose skate was using the relatively minute spatial changes in the temporally constant GMF as a navigational cue. Thus, attunement to GMF stimuli could prime the skate to perceive and respond more readily to constant EMF-DC stimuli such that they further reduce their velocity to avoid

disorientation and maintain their desired bearing. In this case, the constant EMF-DC stimulus might not swamp the electro- or magneto- sensory system of skates nor prevent them from detecting the relatively small signal of GMF displacement. Conversely, the large fluctuating EMF-AC stimuli could overstimulate the sensory systems of skates and prompt them to vacate the general area with an elevated velocity. Exposing free ranging elasmobranchs in large tanks to various levels of EMF-AC and EMF-DC could determine the minimum thresholds and detection distances of stimuli and generate EMF dose-response curves that describe how behavioral responses vary with dosage. Future studies that aim to answer these questions could build on our results and further our understanding of how magnetic stimuli are detected by various species, and which species would be the most suitable sentinels to elucidate the impacts of anthropogenic EMF on marine fauna.

ACKNOWLEDGEMENTS

The authors would like to acknowledge Tom Hurst (Alaska Fisheries Science Center, NOAA) for donating experimental and husbandry facilities, Bryson Robertson (Pacific Marine Energy Center at Oregon State University), Richard Shore (F/V Lady Kathy) and Yogi Briggs (R/V Oceanus) for collecting skates, Steve Vogel and Jim Burke of the Oregon Coast Aquarium, and Trevor Erdman and Sid Stetson of the Hatfield Marine Science Center Visitor's Center for donating skates and husbandry support; Chris Rowe, Kyra Kappos, Marie Schlaf, Joshua Bowman, Devon Guerrero, and Maddie English for husbandry support; Baxter Milsap, Rylin Duster, Bob Davidson, and Drummond Wengrove for support in the design and construction of experimental equipment.

COMPETING INTERESTS

The authors declare no competing interests.

FUNDING

This project was supported by a 2022-2024 Biennial Research Grant from Oregon Sea Grant (#NA22OAR4170102), and the Pacific Marine Energy Center at Oregon State University.

DATA AVAILABILITY

All datasets, R scripts with detailed analyses, and code are available on the Open Science Framework repository, https://osf.io/azydm/

SUPPLEMENTAL INOFRMATION

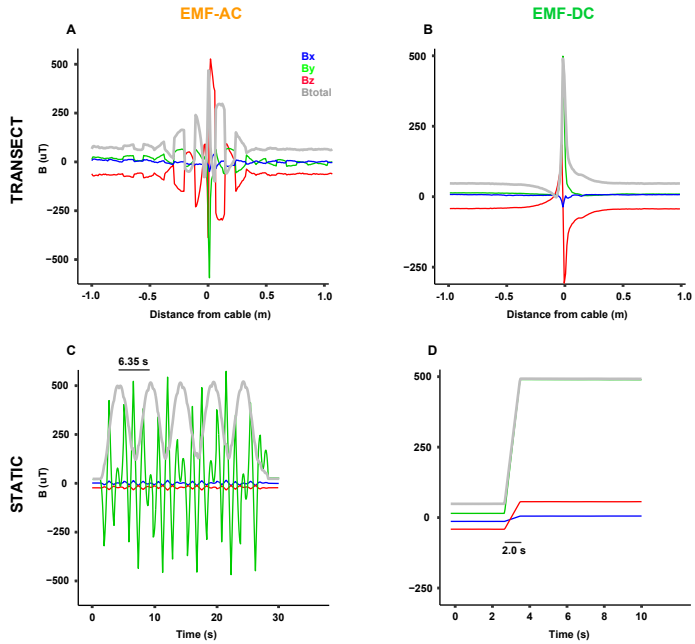

FIGURE S-1.

Figure SI-1. The EMF emitted by AC cables varied with space and time, whereas the EMF from DC cables varied with space. Transects of a tri-axial magnetometer from south (left) to north (right) along the bottom of the experimental tank (2 m diameter) depict how EMF noise stimuli from (a) fluctuating AC and (b) constant DC electric cables vary with distance from the mock subsea cable located directly beneath the tank along the central west-east axis (0 m). Continuous magnetometer readings from directly over the mock cable shows the total strength of EMF stimuli from c) 60Hz AC electrical current fluctuates at an overall frequency of 0.157 Hz, whereas the EMF from d) DC electrical current has a 2.0 s onset to reach a constant value. The total EMF stimulus strength (gray lines; B_{total}) was the vector sum of the X (blue line; B_x), Y (green line: B_y), and Z (red line: B_z) components. The total strength of EMF stimuli were 10X (AC = ± 510 μT; DC = + 510 μT) that of the ambient geomagnetic field (51 μT). All magnetometer readings were recorded at 10 Hz with the +X-axis oriented to the east, the +Y-axis to the north, and +Z-axis was upward.

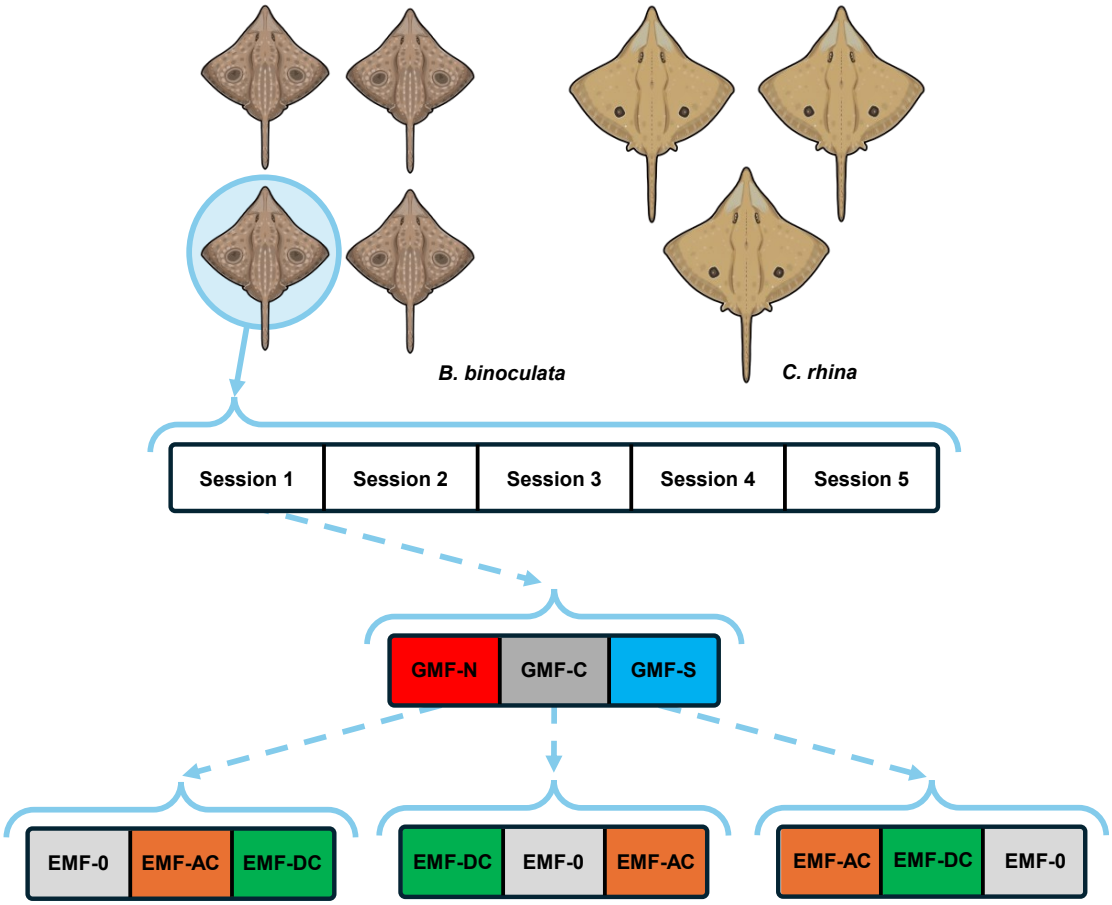

Figure SI-2. Nested block (repeated measures) experimental design of skates exposed to GMF and EMF stimuli. During one session, each skate underwent nine different magnetic treatments that consisted of three electromagnetic exposure treatments (e.g., EMF-0 (control, no EMF), EMF-AC (from an AC cable), and EMF-DC (from a DC cable)), under three different geomagnetic conditions (e.g., GMF-C (control, ambient GMF), GMF-N (GMF displacement to a northern geographic location), and GMF-S (GMF displacement to a southern geographic location)). Sessions were repeated five times for a total of 45 magnetic exposures per skate.

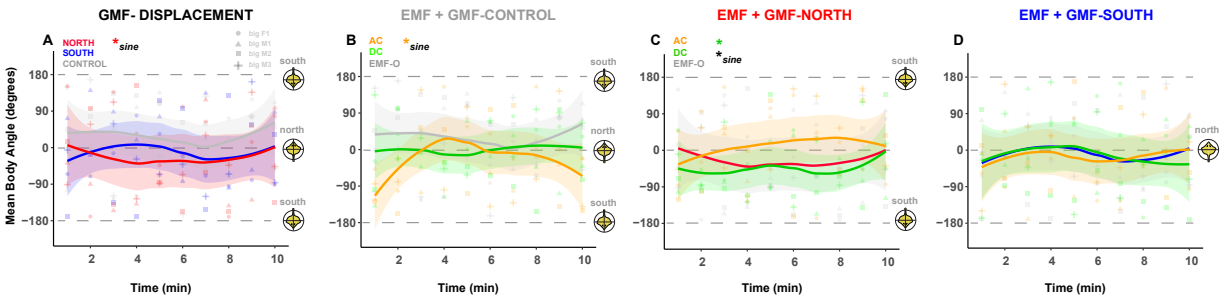

714 **FIGURE S-3.**

715 **Figure SI-3 The mean body angle of big skates during exposure to GMF displacement, EMF alone, and EMF during GMF**
716 **displacement**. Big skates had: A) a significantly different *sine* of their mean body angle (i.e., opposite / hypotenuse) during control
717 trials (gray) compared to GMF-N (red) but not GMF-S (blue) displacement trials; B) a significantly different *sine* of their mean body
718 angle during control trials (gray) compared to EMF-AC (orange) but not EMF-DC (green) trials under ambient GMF (control); C) a
719 significantly different *sine* of their mean body angle during EMF-DC (green) trials compared to control trials (gray) and EMF-AC
720 (orange) trials under GMF-N displacement; and D) no significant difference in mean body angle among EMF-AC trials (orange),
721 EMF-DC (green), and control (red) trials under GMF-S displacement. There were no significant differences in the *cosine* of their
722 mean body angle under any conditions. Control trials (red and blue lines) during (C) GMF-N and (D) GMF-S displacement are the
723 same as those of (A) GMF displacement without EMF. Note that circular data are depicted in a linear fashion, thus the top and
724 bottom dotted lines (i.e., "south") of each panel indicate where the data wraps from top to bottom. Significance values: # = 0.1, * =
725 0.05, ** = 0.01, *** = 0.001. Red symbols compare GMF-N to GMF controls, blue symbols compare GMF-S to GMF controls, orange
726 symbols compare EMF-AC to EMF-0, green symbols compare EMF-DC to EMF-0, black symbols compare EMF-AC to EMF-DC.
727

728

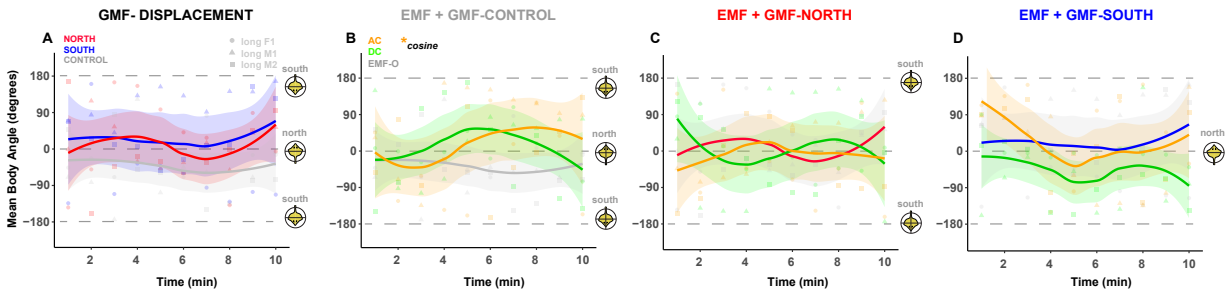

729 **FIGURE S-4.**

730 **Figure SI-4. The mean body angle of longnose skates during exposure to GMF displacement, EMF alone, and EMF during**
731 **GMF displacement**. Longnose skates had: A) no significant difference in mean body angle during control trials (gray) compared to
732 GMF-N (red) or GMF-S (blue) displacement trials; B) a significantly different co*sine* of their mean body angle (i.e., adjacent /
733 hypotenuse) during control trials (gray) compared to EMF-AC (orange) but not EMF-DC (green) trials under ambient GMF (control);
734 C) no significant difference in mean body angle among EMF-AC trials (orange), EMF-DC (green), and control (red) trials under
735 GMF-N displacement; and D) no significant difference in mean body angle among EMF-AC trials (orange), EMF-DC (green), and
736 control (red) trials under GMF-S displacement. There were no significant differences in the *sine* of their mean body angle under any
737 conditions. Control trials (red and blue lines) during (C) GMF-N and (D) GMF-S displacement are the same as those of (A) GMF
738 displacement without EMF. Note that circular data are depicted in a linear fashion, thus the top and bottom dotted lines (i.e., "south")
739 of each panel indicate where the data wraps from top to bottom. Significance values: # = 0.1, * = 0.05, ** = 0.01, *** = 0.001. Red
740 symbols compare GMF-N to GMF controls, blue symbols compare GMF-S to GMF controls, orange symbols compare EMF-AC to
741 EMF-0, green symbols compare EMF-DC to EMF-0, black symbols compare EMF-AC to EMF-DC.
742

743

LITERATURE CITED

Adrianov, G. N., Brown, H. R., & Ilyinsky, O. B. (1974). Responses of central neurons to electrical and magnetic stimuli of the ampullae of Lorenzini in the Black Sea skate. Journal of Comparative Physiology, 93, 287–299.

Adrianov, G. N., Brown, H. R., Ilyinsky, O. B., & Muraveiko, V. M. (1984). Frequency characteristics of skate electroreceptive central neurons responding to electrical and magnetic stimulation. Neirofiziologiya, 16,464–470.

Akoev, G. N., Ilyinsky, O. B., & Zadan, P. M. (1976). Responses of electroreceptors (ampullae of Lorenzini) of skates to electric and magnetic fields. Journal of Comparative Physiology, 106, 127–136.

Albert L, Deschamps F, Jolivet A, Olivier F, Chauvaud L, Chauvaud S. (2020). A current synthesis on the effects of electric and magnetic fields emitted by submarine power cables on invertebrates. Marine Environmental Research, Volume 159. 2020, 104958, ISSN 0141-1136, https://doi.org/10.1016/j.marenvres.2020.104958.

Albert L, Olivier F, Jolivet A, Chauvaud L, and Chauvaud S. (2021). Insights into the behavioural responses of juvenile thornback ray *Raja clavata* to alternating and direct current magnetic fields ," J. Fish Biol., pp. 0–3.

Anderson, J. M., Clegg, T. M., Véras, L. V. M. V. Q., & Holland, K. N. (2017). Insight into shark magnetic field perception from empirical observations. Scientific Reports, 7, 11042. https://doi.org/10.1038/s41598-017-11459-8.

Ball, R. E., Oliver, M. K., & Gill, A. B. (2015). Early life sensory ability— Ventilatory responses of thornback ray embryos (*Raja clavata*) to predator-type electric fields. Developmental Neurobiology, 76, 721–729.

Bedore CN & Kajiura SM. (2013) Bioelectric fields of marine organisms: voltage and frequency contributions to detectability by electroreceptive predators. Physiological and Biochemical Zoology 86

Bevelhimer MS, Cada GF, Fortner AM , Schweizer PE & Riemer K. (2013). Behavioral Responses of Representative Freshwater Fish Species to Electromagnetic Fields, Transactions of the American Fisheries Society, 142:3, 802-813, DOI:10.1080/00028487.2013.778901

Brown, H. R., & Ilyinsky, O. B. (1978). The ampullae of Lorenzini in the magnetic field. Journal of Comparative Physiology, 126, 333–341.

Copping, A.E. and Hemery, L.G., editors 2020. OES-Environmental State of the Science Report: Environmental Effects of Marine Renewable Energy Development Around the World. Report for Ocean Energy Systems (OES). doi:10.2172/1632878.

Desender, M., Kajiura, S., Ampe, B., Dumolein, L., Polet, H., Chiers, K., & Decostere, A. (2017). Pulse trawling: evaluating its impact on prey detection by small-spotted catshark (*Scyliorhinus canicula*). Journal of Experimental Marine Biology and Ecology, 486, 336–343.

Fisher C, and Slater M. 2010. Electromagnetic Field Study: Effects of Electromagnetic Fields on Marine Species: A Literature Review. Oregon Wave Energy Trust. 0905-00-001.

Fuss T, Bleckmann H, Schluessel V (2014) Visual discrimination abilities in the grey bamboo shark, *Chiloscyllium griseum*. Zoology 117:104–111

Fuss T, Russnak V, Stehr K, Schluessel V (2017) World in motion: perception and discrimination of movement in juvenile grey bamboo sharks (*Chiloscyllium griseum*). Anim Behav Cogn 4(3):223–241. https ://doi.org/10.26451 /abc.04.03.03.2017

Gill AB, Gloyne-Phillips I, Kimber J, Sigray P. (2014). Marine renewable energy, electromagnetic (EM) fields and EM-sensitive animals. Pages 61-80 in MA Shields and AIL. Payne (Editors). Marine renewable energy technology and environmental interactions. Springer, Dordrecht, Netherlands.

Gill AB, Huang Y, Gloyne-Philips I, Metcalfe J, Quayle V, Spencer J, Wearmouth V. COWRIE 2.0 Electromagnetic Fields (EMF) Phase 2: EMF-sensitive fish response to EM emissions from sub-sea electricity cables of the type used by the offshore renewable energy industry. Commissioned by COWRIE Ltd (project reference COWRIE-EMF-1-06). 2009 Apr;68.

Gill, A.B., Huang, Y., Spencer, J. & Gloyne-Phillips, I. (2012b) Electromagnetic fields emitted by high voltage alternating current offshore wind power cables and interactions with marine organisms. Institution of engineering and technology, IET electromagnetics in current and emerging and power systems, University of Liverpool, UK.

Gill AB, & Desender M (2020). Risk to animals from electromagnetic fields emitted by electric cables and marine renewable energy devices. Pp. 86–103 in OES-Environmental 2020 State of the Science Report: Environmental Effects of Marine Renewable Energy Development Around the World. No. PNNL-29976CHPT5 Pacific Northwest National Lab, Richland, WA, 18 pp., https://doi.org/10.2172/1633088.

Grew M, Raoult V, Gaston TF (2024). Behavioural response of benthic elasmobranchs to a neodymium magnet under controlled laboratory conditions, Fisheries Research, Volume 271, 2024, 106926, ISSN 0165-7836, https://doi.org/10.1016/j.fishres.2023.106926.

Hermans A, Winter HV, Gill AB, Murk AJ (2024). Do electromagnetic fields from subsea power cables effect benthic elasmobranch behaviour? A risk-based approach for the Dutch Continental Shelf, Environmental Pollution, Volume 346, 2024, 123570, ISSN 0269-7491, https://doi.org/10.1016/j.envpol.2024.123570.

Hutchison ZL, Sigray P, He H, Gill AB, King J, and C. Gibson C, (2018). Electromagnetic Field (EMF) Impacts on Elasmobranch (shark, rays, and skates) and American Lobster Movement and Migration from Direct Current Cables. Sterling (VA): U.S. Department of the Interior, Bureau of Ocean Energy Management. OCS Study BOEM 2018-003.

Hutchison ZL, Gill AB, P Sigray, H He, JW King (2020). Anthropogenic electromagnetic fields (EMF) influence the behaviour of bottom-dwelling marine species. Scientific Reports 10(1):4219, https://doi.org/10.1038/s41598-020-60793-x.

Hutchison ZL, Secor DH & Gill AB. (2021). The interaction between resource species and electromagnetic fields associated with electricity production by offshore wind farms. Oceanography 33(4):96–107

Kalmijn, A. D. (1978). Experimental evidence of geomagnetic orientation in elasmobranch fishes. In K. Schmidt-Koening &W. T. Keaton (Eds.), Animal migration, navigation and homing (pp. 347–353). Berlin, Germany: Springer-Verlag.

Kalmijn, A. J. (1981). Biophysics of geomagnetic field detection. IEEE Transactions on Magnetism, 17, 1113–1124.

Kalmijn, A. J. (1982). Electric and magnetic field detection in elasmobranch fishes. Science, 218, 916–~~918.~~

Kalmijn, A. J. (1984). Theory of electromagnetic orientation: A further analysis. In L. Bolis, R. D. Keynes, & S. H. P. Madrell (Eds.), Comparative physiology of sensory systems (pp. 525–560). Cambridge, UK: Cambridge University Press.

Kalmijn, A. J. (2000). Detection and processing of electromagnetic and near-field acoustic signals in elasmobranch fishes. Philosophical Transactions of the Royal Society B, 355, 1135–1141.

Kajiura SM, Holland KN, 2002. Electroreception in juvenile scalloped hammerhead and sandbar sharks. J. Exp. Biol. 205, 3609–3621.

Keller BK, Putman N, Grubbs RD, Portnoy DS, Murphy TS. (2021). Map-like use of Earth's magnetic field in sharks, Current Biology (2021), https://doi.org/10.1016/j.cub.2021.03.103

Kempster, R. M., Hart, N. S., & Collin, S. P. (2012). Survival of the stillest: predator avoidance in shark embryos. PLoS One, 8, e52551.

Klimley, A.P., 1993. Highly directional swimming by scalloped hammerhead sharks, *Sphyrna lewini*, and subsurface irradiance, temperature, bathymetry, and geomagnetic field. Mar. Biol. 117 (1), 1–22. https://doi.org/10.1007/BF00346421.

Klimley AP, Putman NF, Keller B, and Noakes D. 2021. Does EMF from subsea cables alter the migrations of marine animals? Conservation Science and Practice. DOI:10.1111/csp2.436.

Lauer, J., Zhou, M., Ye, S. *et al.* Multi-animal pose estimation, identification and tracking with DeepLabCut. *Nat Methods* 19, 496–504 (2022). https://doi.org/10.1038/s41592-022-01443-0

Marra, L.J., 1989. Sharkbite on the SL submarine lightwave cable system: history, causes, and resolution. IEEE J. Ocean. Eng. 14 (3), 230–237. https://doi.org/10.1109/48.29600.

Meyer, C. G., Holland, K. N., & Papastamatiou, Y. P. (2005). Sharks can detect changes in the geomagnetic field. Journal of the Royal Society Interface, 2, 129–130.

Minkoff, D., Putman, N. F., Atema, J., & Ardren, W. R. (2020). Nonanadromous and anadromous Atlantic salmon differ in orientation responses to magnetic displacements. *Canadian journal of fisheries and aquatic sciences*, *77*(11), 1846-1852.

Molteno, T.C.A., Kennedy, W.L., 2009. Navigation by induction-based magnetoreception in elasmobranch fishes. Journal of Biophysics 1–6. https://doi.org/10.1155/2009/380976, 2009.

Montgomery, J. C. (1984). Frequency response characteristics of primary and secondary neurons in the electrosensory neurons in the electrosensory system of the thornback ray. Comparative Biochemistry and Physiology A, 79, 189–195.

Murray, R. W. (1962). The response of the ampullae of Lorenzini in elasmobranchs to electrical stimulation. Journal of Experimental Biology, 39, 119–128.

Naisbett-Jones, L.C., Putman, N.F., Stephenson, J.F., Ladak, S. and Young, K.A., 2017. A magnetic map leads juvenile European eels to the Gulf Stream. Current Biology, 27(8), pp.1236-1240.

Naisbett-Jones, L. C., Putman, N. F., Scanlan, M. M., Noakes, D. L., & Lohmann, K. J. (2020). Magnetoreception in fishes: the effect of magnetic pulses on orientation of juvenile Pacific salmon. *Journal of Experimental Biology*, *223*(10), jeb222091.

Newton KC & Kajiura SM. (2017). Magnetic field discrimination, learning, and memory in the yellow stingray, *Urobatis jamaicensis*. Animal Cognition. 20(4): 603-614. doi.org/10.1007/s10071-017-1084-8

Newton KC & Kajiura SM. (2020a). The yellow stingray, *Urobatis jamaicensis*, can use magnetic field polarity to orient in space and solve a maze. Marine Biology. 167:36. doi.org/10.1007/s00227-019-3643-9

Newton KC & Kajiura SM. (2020b). The yellow stingray, *Urobatis jamaicensis*, can discriminate the geomagnetic cues necessary for a bicoordinate magnetic map. Marine Biology. 167:151. doi.org/10.1007/s00227-020-03763-1

Newton KC, Kacev D, Nilsson SRO, Saettele A, Golden SA & Sheets L. (2023). Lateral Line Ablation by Ototoxic Compounds Results in Distinct Rheotaxis Profiles in Larvae Zebrafish. Communications Biology. 6:84. doi.org/10.1038/s42003-023-04449-2

Nyqvist, D., Durif, C., Johnsen, M.G., De Jong, K., Forland, T.N., Sivle, L.D., 2020. Electric and magnetic senses in marine animals, and potential behavioral effects of electromagnetic surveys. Mar. Environ. Res. 155, 104888 https://doi.org/10.1016/j. marenvres.2020.104888

Orr M (2016). The potential impacts of submarine power cables on benthic elasmobranchs, Doctoral thesis. University of Auckland Research.

O'Connell, C. P., Abel, D. C., Rice, P. H., Stroud, E. M., & Simuro, N. C. (2010). Responses of the southern stingray (*Dasyatis americana*) and the nurse shark (*Ginglymostoma cirratum*) to permanent magnets. Marine and Freshwater Behaviour and Physiology, 43, 63–73.

O'Connell, C. P., Gruber, S. H., Abel, D. C., Stroud, E. M., & Rice, P. H. (2011b). The responses of juvenile lemon sharks, *Negaprion brevirostris*, to a magnetic barrier. Ocean & Coastal Management, 54, 225–230.

O'Connell, C. P., Andreotti, S., Rutzen, M., Meyer, M., & He, P. (2014a). The use of permanent magnets to reduce elasmobranch encounter with a simulated beach net. 2. The great white shark (*Carcharodon carcharia*s). Ocean & Coastal Management, 97, 20–28.

O'Connell, C. P., Guttridge, T. L., Brooks, J., Finger, J. S., Gruber, S. H., & He, P. (2014b). Behavioural modification of visually deprived lemon sharks (*Negaprion brevirostris)* towards magnetic fields. Journal of Experimental Marine Biology & Ecology, 453, 131–137.

O'Connell, C. P., Hyun, S. Y., Gruber, S. H., O'Connell, T. J., Johnson, G., Grudecki, K., & He, P. (2014c). The use of permanent magnets to reduce elasmobranch encounter with a simulated beach net. 1. The bull shark (*Carcharhinus leucas*). Ocean & Coastal Management, 97, 12–19.

O'Connell, C. P., Hyun, S. Y., Gruber, S. H., & He, P. (2015). Effects of barium-ferrite permanent magnets on great hammerhead shark *Sphyrna mokarran* behaviour and implications for future conservation technologies. Endangered Species Research, 26, 243–256.

Paulin, M. G. (1995). Electrorecpetion and the compass sense of sharks. Journal of Theoretical Biology, 174, 325–339.

Peters, R. C., & Evers, H. P. (1985). Frequency selectivity in the ampullary system of an elasmobranch fish (*Scyliorhinus canicula*). The Journal of Experimental Biology, 118, 99–109.

Polpetta, M., Piva, F., Gridelli, S., Bargnesi, F., (2021). Behavioural responses in the sand tiger shark (*Carcharias taurus*) to permanent magnets and pulsed magnetic fields. Mar. Biol. Res. 17 (1), 41–56. https://doi.org/10.1080/17451000.2021.1887496.

Richards RJ, Raoult V, Powter DM & Gaston TF. (2018) Permanent magnets reduce bycatch of benthic sharks in an ocean trap fishery, Fisheries Research 208, 16-21.

Robbins, W. D., Peddemors, V. M., & Kennelly, S. J. (2011). Assessment of permanent magnets and electropositive metals to reduce the line-based capture of Galapagos sharks, *Carcharhinus galapagensis*. Fisheries Research, 109, 100–106.

Schluessel V, Beil O, Weber T, Bleckmann H (2014) Symmetry perception in bamboo sharks (*Chiloscyllium griseum*) and Malawi cichlids (*Pseudotropheus sp.*). Anim Cogn 17(5):1187–1205

Scott K, Harsanyi P, Easton BAA, Piper AJR, Rochas CMV, Lyndon AR (2021) Exposure to Electromagnetic Fields (EMF) from Submarine Power Cables Can Trigger Strength-Dependent Behavioural and Physiological Responses in Edible Crab, Cancer pagurus (L.). J. Mar. Sci. Eng. 9:776 https://doi.org/10.3390/jmse9070776

Siegenthaler A, Niemantsverdriet PRW, Laterveer M, Heitkönig IMA. (2016) Aversive responses of captive sandbar sharks Carcharhinus plumbeus to strong magnetic fields. Journal of Fish Biology 89, 0022-1112.

Sisneros, J. A., & Tricas, T. C. (2000). Androgen-induced changes in response dynamics of primary ampullary electrosensory primary afferent neurons. Journal of Neuroscience, 20, 8586–8595.

Sisneros, J. A., & Tricas, T. C. (2002). Ontogenetic changes in the response properties of the peripheral electrosensory system in the Atlantic stingray (*Dasyatis sabina*). Brain Behaviour and Evolution, 59, 130–140.

Sisneros, J. A., Tricas, T. C., & Luer, C. A. (1998). Response properties and biological function of the skate electrosensory system during ontogeny. Journal of Comparative Physiology A, 183, 87–99.

Slater M, Schultz A, Jones R. (2010). Electromagnetic Field Study: Estimated Ambient Electromagnetic Field Strength in Oregon's Coastal Environment. Oregon Wave Energy Trust. 0905-00-002.

Smith, L. E., & O'Connell, C. P. (2014). The effects of neodymium-ironboron permanent magnets on the behaviour of the small spotted catshark (*Scyliorhinus canicula*) and the thornback skate (Raja clavata). Ocean & Coastal Management, 97, 44–49.

Stoner, A. W., & Kaimmer, S. M. (2008). Reducing elasmobranch bycatch: laboratory investigation of rare earth metal and magnetic deterrents with piked dogfish and Pacific halibut. Fisheries Research, 92, 162–168.

Taormina, B., Bald, J., Want, A., Thouzeau, G., Lejart, M., Desroy, N., & Carlier, A. (2018). A review of potential impacts of submarine power cables on the marine environment: knowledge gaps, recommendations and future directions. Renewable and Sustainable Energy Reviews, 96, 380–391.

Tricas, T. C., & New, J. G. (1998). Sensitivity and response dynamics of elasmobranch electrosensory primary afferent neurons to near threshold fields. Journal of Comparative Physiology A, 182, 89–101.

Woodruff DL, Cullinan VI, Copping AE, and Marshall KE. (2013). Effects of Electromagnetic Fields on Fish and Invertebrates. U.S. Department of Energy. PNNL-22154.

Wyman, M. T., Peter Klimley, A., Battleson, R. D., Agosta, T. V., Chapman, E. D., Haverkamp, P. J., ... & Kavet, R. (2018). Behavioral responses by migrating juvenile salmonids to a subsea high-voltage DC power cable. *Marine Biology*, *165*, 1-15.

Wyman, M.T., Kavet, R., Battleson, R.D. et al. Assessment of potential impact of magnetic fields from a subsea high-voltage DC power cable on migrating green sturgeon, *Acipenser medirostris*. Mar Biol 170, 164 (2023). https://doi.org/10.1007/s00227-023-04302-4

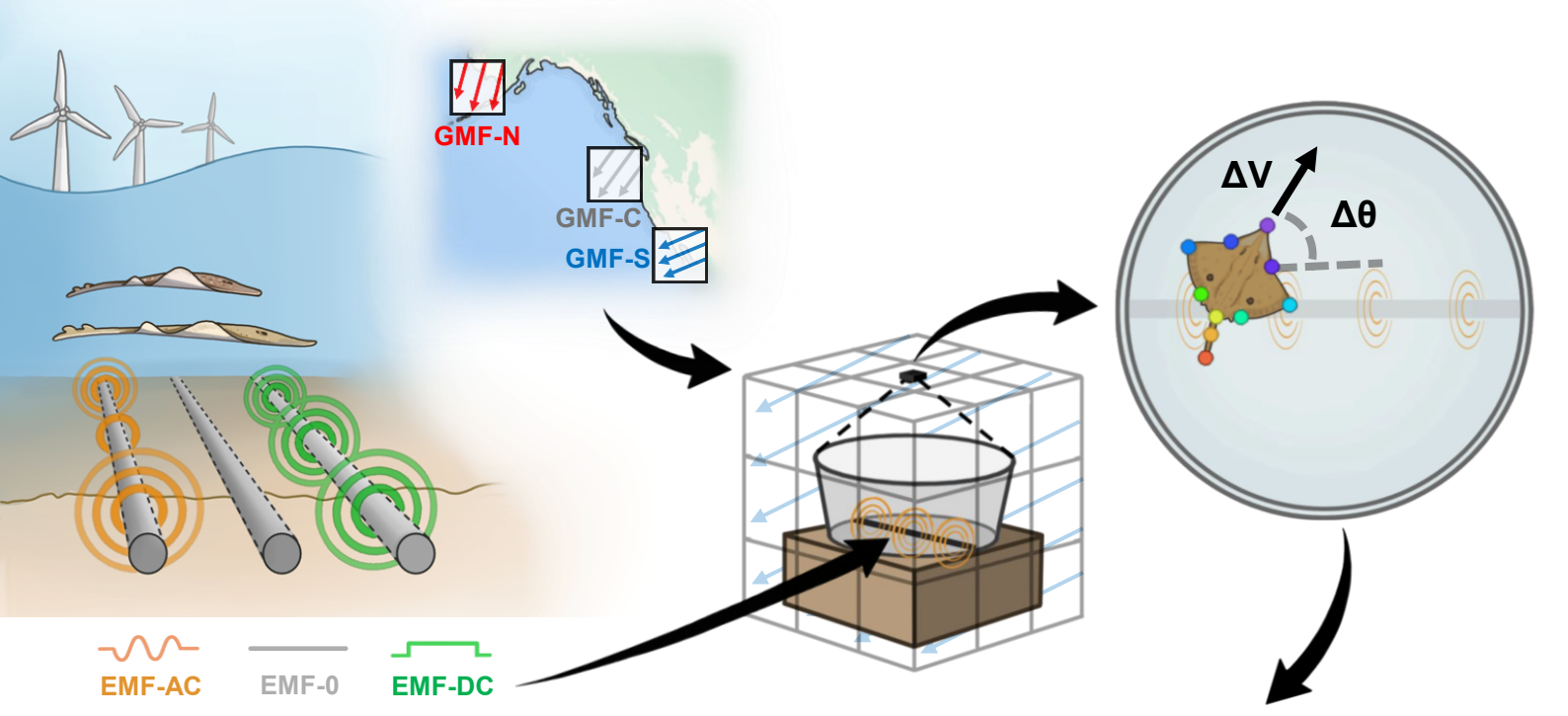
GMF-N
GMF-C
GMF-S
ΔV
Δθ
EMF-AC
EMF-0
EMF-DC

RESULTS

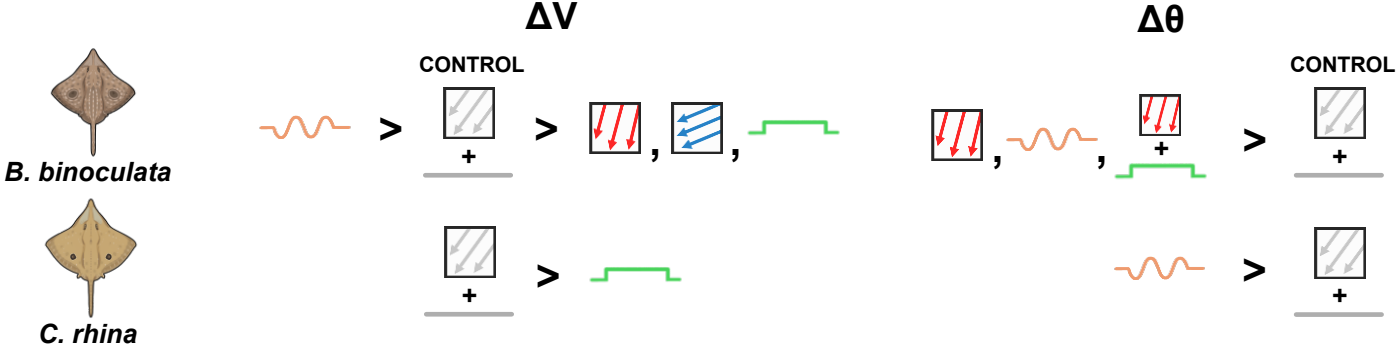
ΔV
Δθ
CONTROL
CONTROL
B. binoculata
C. rhina

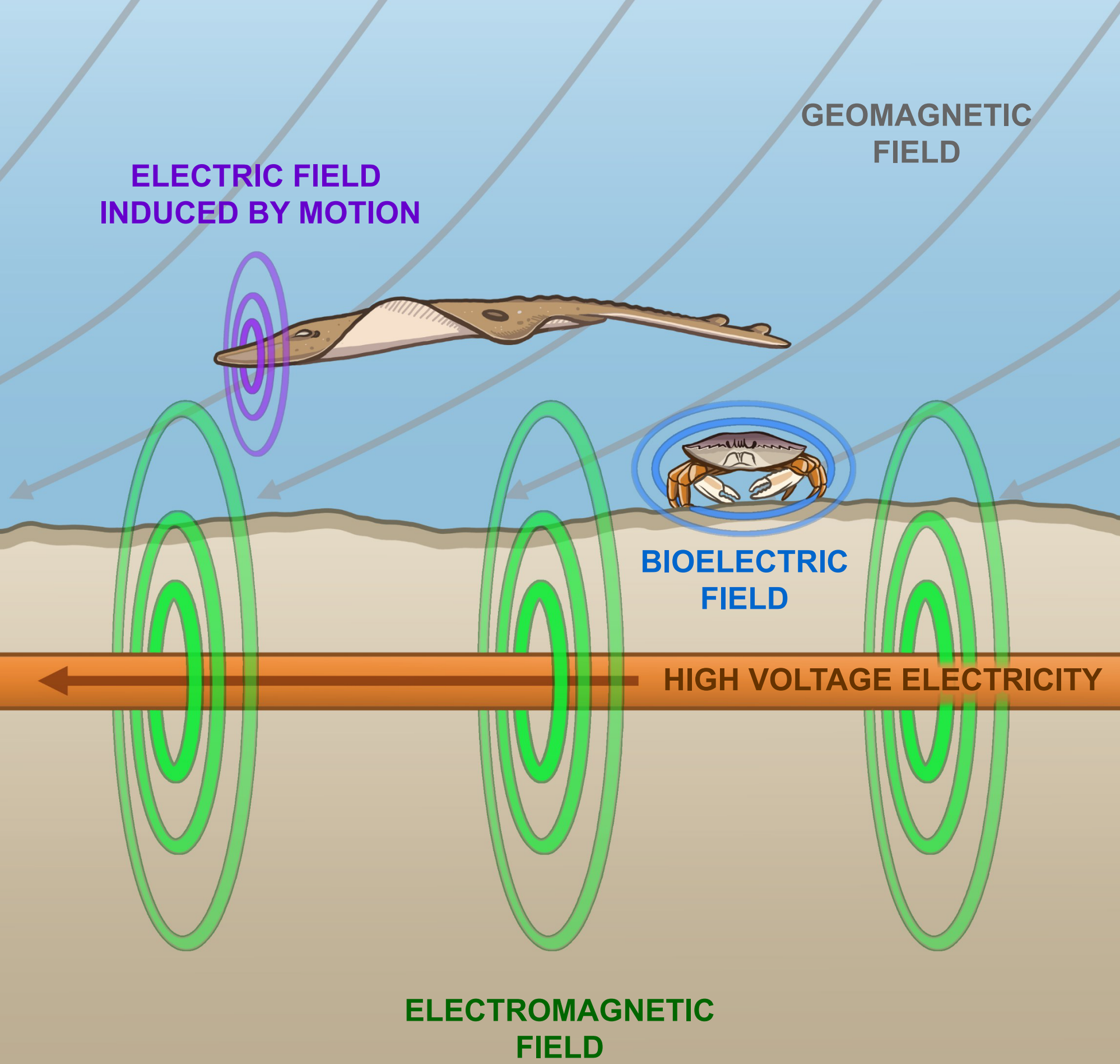
GEOMAGNETIC FIELD
ELECTRIC FIELD INDUCED BY MOTION
BIOELECTRIC FIELD
HIGH VOLTAGE ELECTRICITY
ELECTROMAGNETIC FIELD

FIGURE 1.

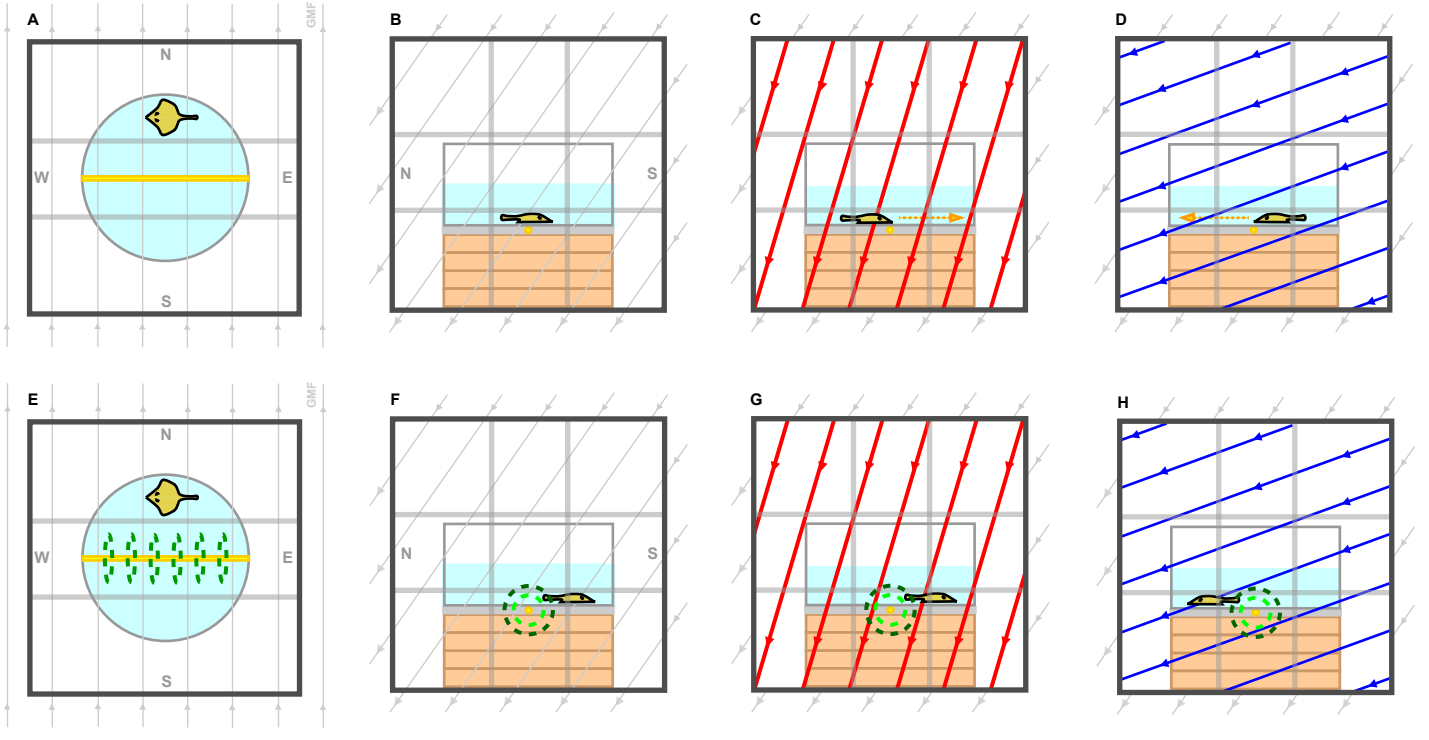

FIGURE 2.

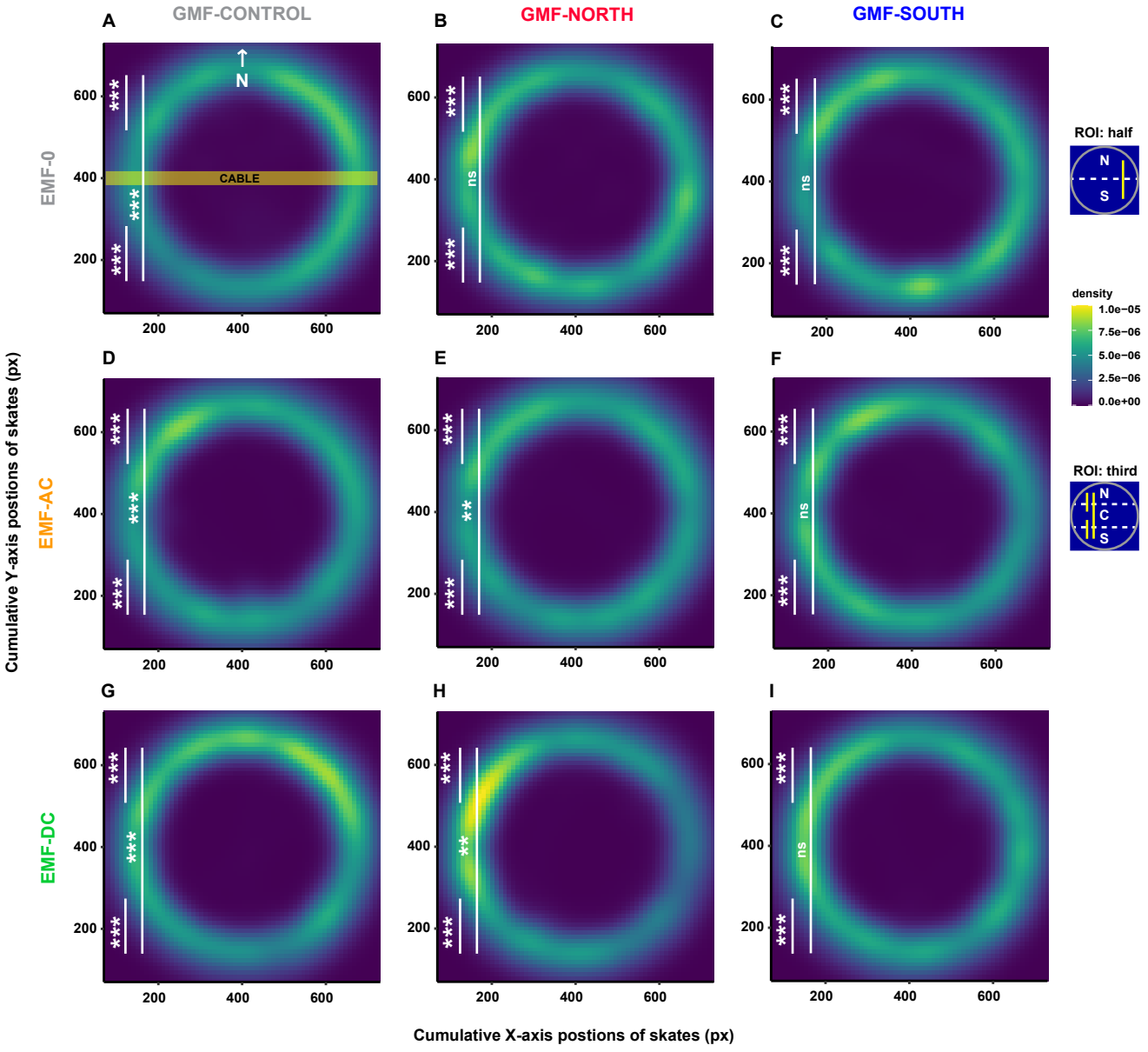
A
GMF-CONTROL
B
GMF-NORTH
C
GMF-SOUTH
D
E
F
G
H
I
EMF-0
EMF-AC
EMF-DC
N
CABLE
***
**
ns
ROI: half
N
S
ROI: third
N
C
S
density
1.0e−05
7.5e−06
5.0e−06
2.5e−06
0.0e+00
Cumulative Y-axis postions of skates (px)
Cumulative X-axis postions of skates (px)
200
400
600

FIGURE 3.

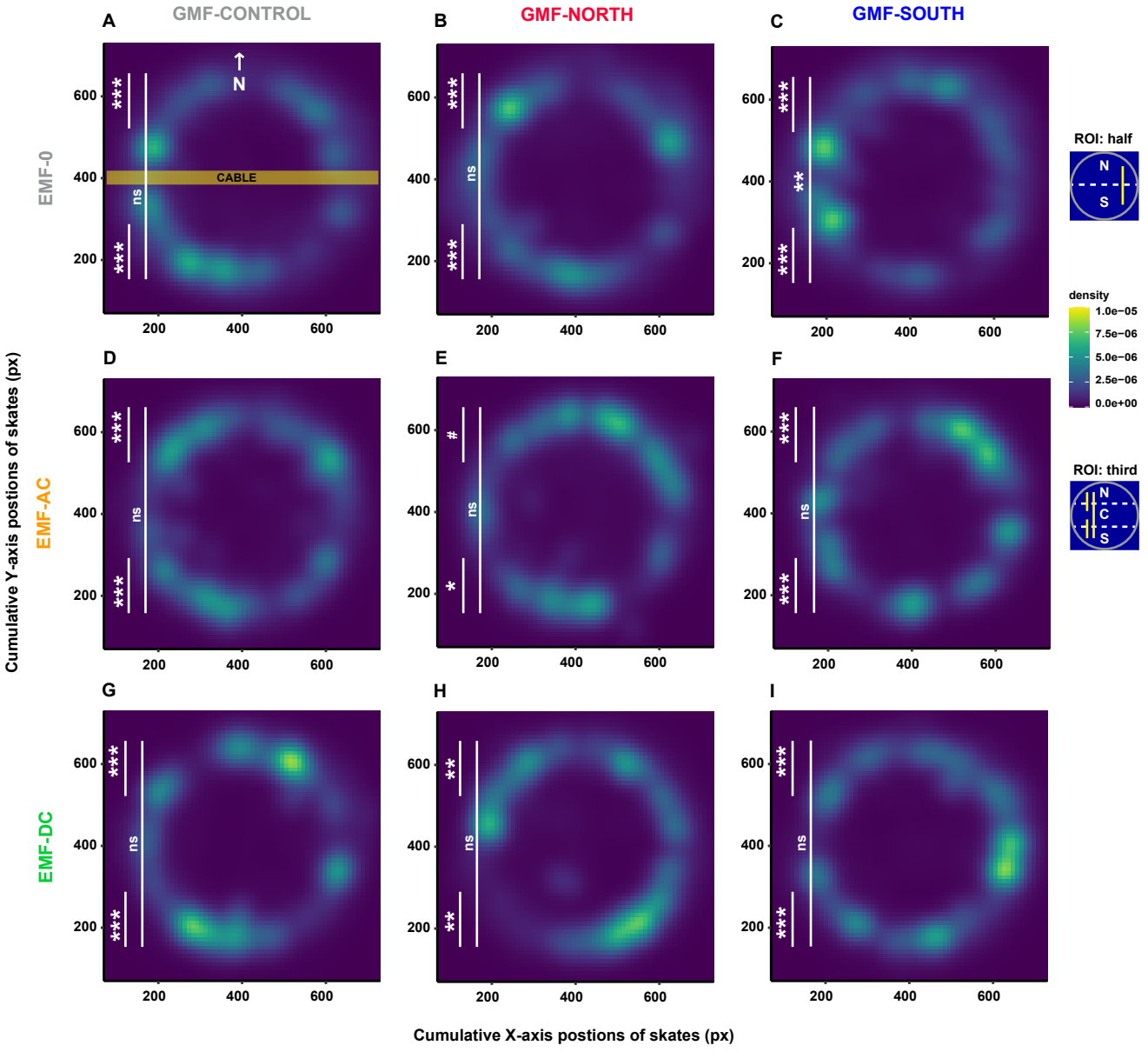
A
GMF-CONTROL
B
GMF-NORTH
C
GMF-SOUTH
D
E
F
G
H
I
EMF-0
EMF-AC
EMF-DC
N
CABLE
***
ns
**
#
*
ROI: half
N
S
ROI: third
N
C
S
density
1.0e−05
7.5e−06
5.0e−06
2.5e−06
0.0e+00
Cumulative Y-axis postions of skates (px)
Cumulative X-axis postions of skates (px)
200
400
600

FIGURE 4.

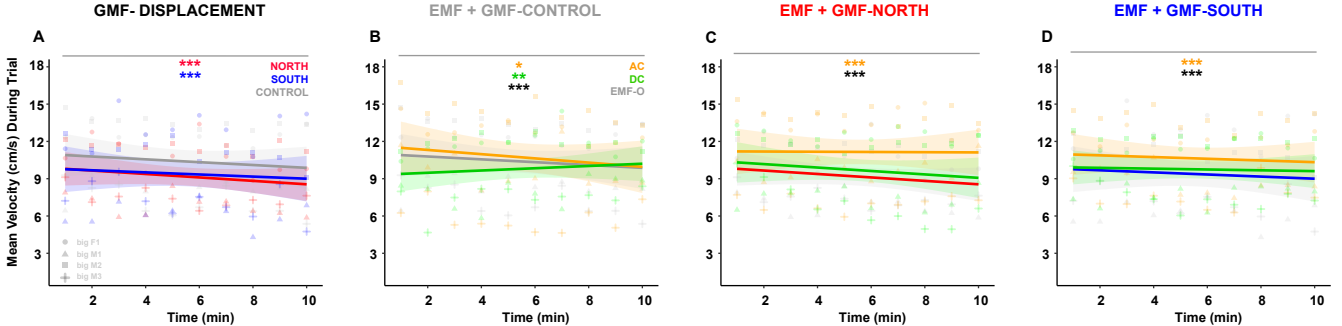
GMF- DISPLACEMENT
EMF + GMF-CONTROL
EMF + GMF-NORTH
EMF + GMF-SOUTH
A
B
C
D
Mean Velocity (cm/s) During Trial
Time (min)
NORTH
SOUTH
CONTROL
AC
DC
EMF-O
big F1
big M1
big M2
big M3

FIGURE 5.

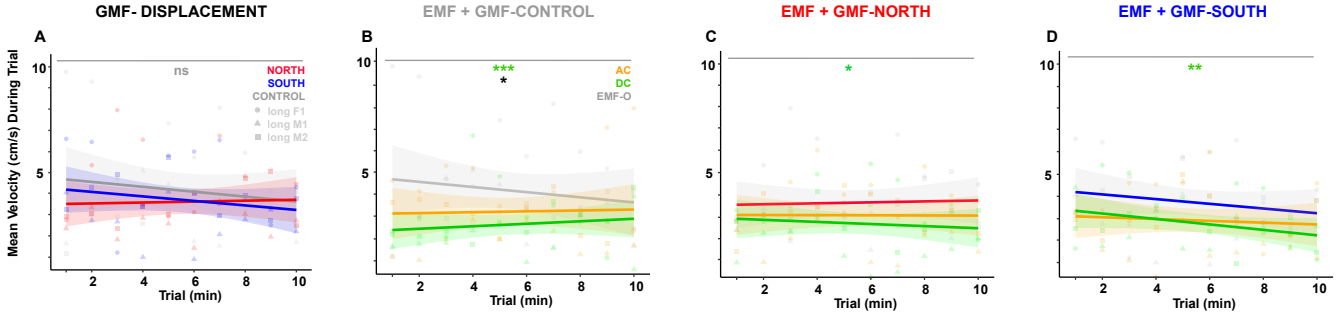
GMF- DISPLACEMENT
EMF + GMF-CONTROL
EMF + GMF-NORTH
EMF + GMF-SOUTH
A
B
C
D
Mean Velocity (cm/s) During Trial
Trial (min)
ns
NORTH
SOUTH
CONTROL
long F1
long M1
long M2
***
*
AC
DC
EMF-O
*
**

FIGURE 6.

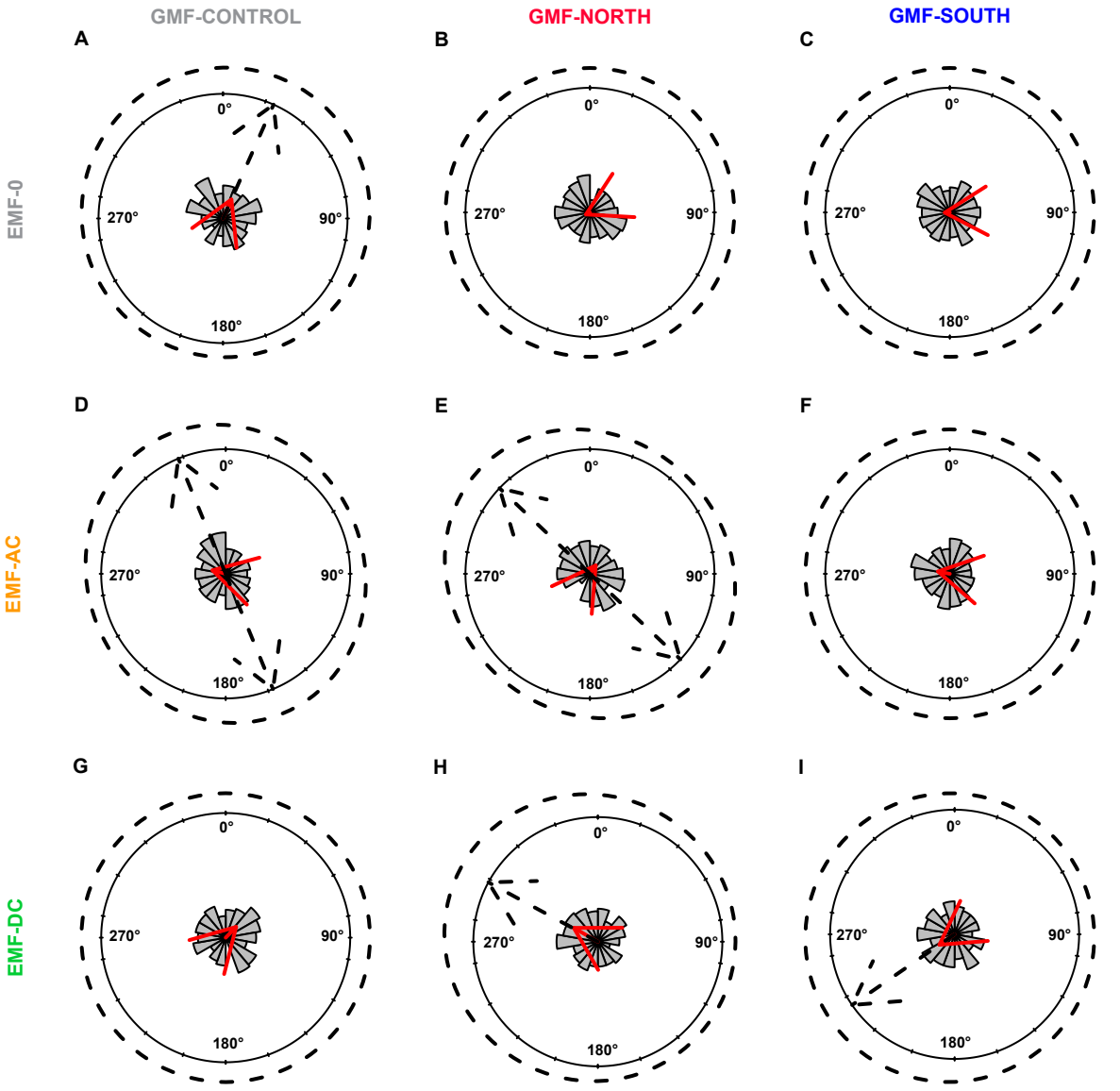
GMF-CONTROL
GMF-NORTH
GMF-SOUTH
EMF-0
EMF-AC
EMF-DC
A
B
C
D
E
F
G
H
I
0°
90°
180°
270°

FIGURE 7.

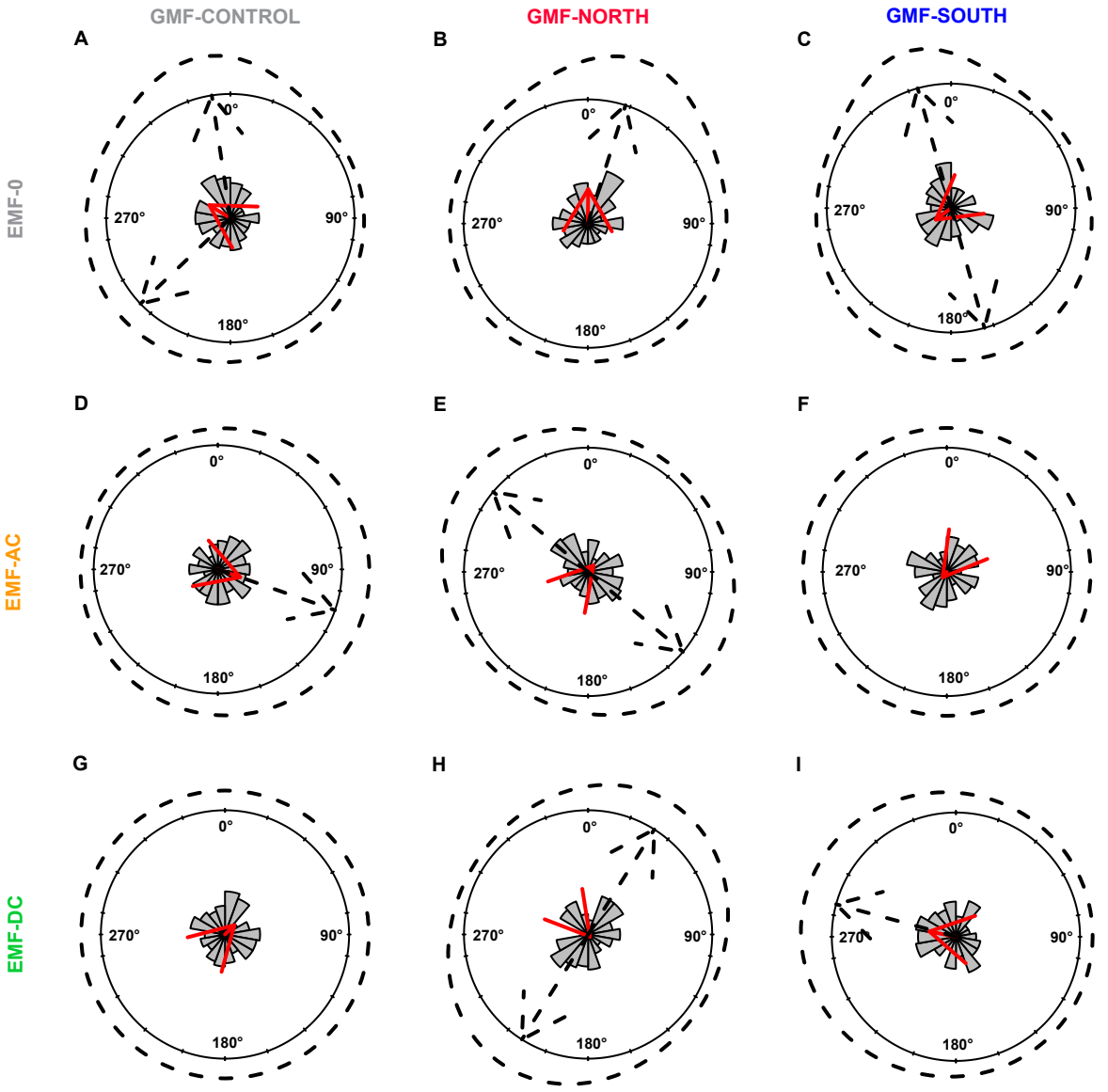
GMF-CONTROL
GMF-NORTH
GMF-SOUTH
EMF-0
EMF-AC
EMF-DC
A
B
C
D
E
F
G
H
I
0°
90°
180°
270°

FIGURE 8.

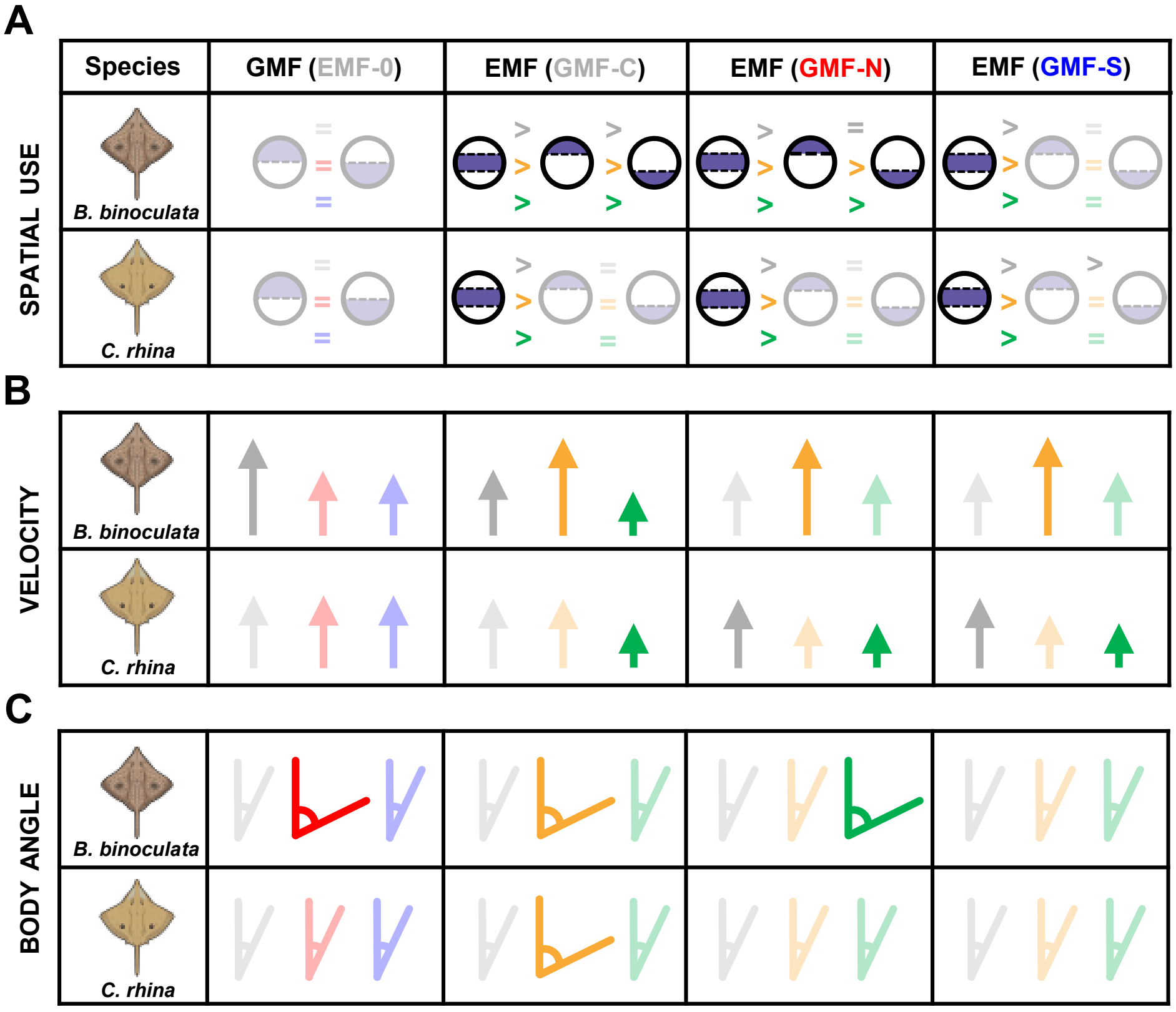
A
Species
GMF (EMF-0)
EMF (GMF-C)
EMF (GMF-N)
EMF (GMF-S)
SPATIAL USE
B. binoculata
C. rhina
B
VELOCITY
B. binoculata
C. rhina
C
BODY ANGLE
B. binoculata
C. rhina

FIGURE 9.